Title: Distal axotomy enhances retrograde presynaptic excitability onto injured pyramidal neurons via trans-synaptic signaling

Authors: Tharkika Nagendran[1,3], Rylan S. Larsen[2,3,8], Rebecca L. Bigler[5], Shawn B. Frost[6,7], Benjamin D. Philpot[2,3,4], Randolph J. Nudo[6,7], Anne Marion Taylor[1,3,4]*

Affiliations:

[1] UNC/NCSU Joint Department of Biomedical Engineering, UNC-Chapel Hill, Chapel Hill, Campus box 7575, NC 27599-7575 USA

[2] Department of Cell Biology and Physiology, UNC-Chapel Hill, Campus box 7545, Chapel Hill, NC 27599-7545 USA

[3] UNC Neuroscience Center, Campus box 7250, UNC-Chapel Hill, Chapel Hill, NC 27599-7250 USA

[4] Carolina Institute for Developmental Disabilities, Campus box 7255, Chapel Hill, NC 27599-7255 USA

[5] Curriculum in Genetics and Molecular Biology, UNC-Chapel Hill, Chapel Hill, NC 27599 USA

[6] Landon Center On Aging, University of Kansas Medical Center, 3901 Rainbow Blvd., Kansas City, KS 66160 USA

[7] Department of Rehabilitation Medicine, University of Kansas Medical Center, 3901 Rainbow Blvd., Kansas City, KS 66160 USA

[8]Present address: Allen Institute for Brain Science, 615 Westlake Ave. N, Seattle, WA 98109, USA

*To whom correspondence should be addressed: anne.marion.taylor@gmail.com

Abstract

Injury of CNS nerve tracts remodels circuitry through dendritic spine loss and hyper-excitability, thus influencing recovery. Due to the complexity of the CNS, a mechanistic understanding of injury-induced synaptic remodeling remains unclear. Using microfluidic chambers to separate and injure distal axons, we show that axotomy causes retrograde dendritic spine loss at directly injured pyramidal neurons followed by retrograde presynaptic hyper-excitability. These remodeling events require activity at the site of injury, axon-to-soma signaling, and transcription. Similarly, directly injured corticospinal neurons *in vivo* also exhibit a specific increase in spiking following axon injury. Axotomy-induced hyper-excitability of cultured neurons coincides with elimination of inhibitory inputs onto injured neurons, including those formed onto dendritic spines. *Netrin-1* downregulation occurs following axon injury and exogenous netrin-1 applied after injury normalizes spine density, presynaptic excitability, and inhibitory inputs at injured neurons. Our findings show that intrinsic signaling within damaged neurons regulates synaptic remodeling and involves netrin-1 signaling.

Introduction

Acquired brain injuries, such as occur in stroke and traumatic brain injury, induce significant synaptic reorganization, even in uninjured cortical regions remote from the site of damage [1-3]. This enhanced neural plasticity supports formation of new connections and expansion of cortical territories, well-described in humans using neuroimaging and non-invasive stimulation techniques [1, 2, 4, 5]. However, the cellular mechanisms of this injury-induced plasticity remain largely unknown.

In healthy brains, long projection neurons with somatodendritic domains housed in cerebral cortex extend axons into numerous distant areas of the CNS, including the spinal cord and the apposing cortical hemisphere. When these remote areas are injured, long projection axons are damaged and injury signals propagate retrogradely to somatodendritic domains. Retrograde injury signal propagation leads to somatic responses such as chromatolysis and new transcription [6, 7]. For example, after damage to corticospinal axons resulting from spinal cord injury, dendritic spines in motor cortex undergo time-dependent changes in morphology including decreased spine density and alterations in spine length and diameter [8]. Loss of local GABAergic inhibition also occurs at somatodendritic regions following injury, which is thought to unmask preexisting excitatory connections and result in enhanced excitability [2, 9, 10]. These findings suggest that a cascade of events occurs following distal axonal injury involving retrograde axon-to-soma signaling and then trans-synaptic signaling from the injured neuron to uninjured presynaptic neurons causing synaptic changes and enhanced excitability.

Due to the heterogeneity and complexity of the CNS, intrinsic neuronal responses to distal axon injury and their contributions to synaptic remodeling remain unclear.

Reduced preparations are necessary for examining neuron-specific responses and provide a more experimentally tractable model system to identify and screen drugs to improve neuronal function following injury. Microfluidic chambers are useful for compartmentalization of many types of neurons, including cortical and hippocampal neurons, and allow axons to be injured and manipulated without physically disturbing the proximal neurons housed within the chamber's somatodendritic compartment [11-13]. Because brain injury and disease preferentially affect long projection neurons within the CNS [14, 15], we sought to determine the progression of events that occur intrinsically in these neurons following distal axotomy that lead to synaptic remodeling.

Here we show that axotomized pyramidal neurons underdo dendritic spine loss followed by a transsynaptic enhancement in presynaptic excitability. We find that directly injured neurons preferentially exhibit enhanced excitability and our evidence suggests that these synaptic remodeling events require retrograde signaling from the site of axon injury to the nucleus to rapidly activate transcription. Loss of inhibitory inputs coincides with enhanced presynaptic excitability. We identified *netrin-1* as significantly downregulated following axotomy and found that application of exogenous netrin-1 protein several hours after axotomy, restored spine density and normalized presynaptic excitability, including the fraction of inhibitory inputs onto injured neurons.

Results

In vitro model to study axon injury of pyramidal neurons

To investigate how distal axon injury remodels synapses contacting injured

neurons, we used a microfluidic approach to compartmentalize cultured neurons. Microfluidic chambers containing microgroove-embedded barriers approximately 900 µm in length were used to compartmentalize axons independently from dendrites and somata of rat central neurons as demonstrated previously (**Supplementary Fig. 1a**) [11, 12, 16]. Using this approach we subjected neurons to distal axotomy ~1 mm away from their physically undisturbed dendrites and somata [11, 16]. We used hippocampal neurons harvested from embryonic rats to generate a more consistent, enriched population of pyramidal neurons (85-90% pyramidal) compared with similarly harvested cortical neurons. Further, hippocampal neurons exhibit morphology characteristic of maturing pyramidal neurons *in vivo* [17]; the remaining hippocampal neurons are mostly inhibitory GABAergic interneurons [18]. To identify neurons with axons projecting into the axonal compartment, we retrogradely labeled neurons by applying a G-deleted rabies virus expressing fluorescent proteins (incompetent for trans-synaptic transfer) to the axonal compartment and characterized the morphology of the labeled neurons. We found that 94% (42 of 45) of virally-labeled neurons were pyramidal neurons and the remaining were unclassifiable (**Fig. 1a**). When these neurons were cultured within the microfluidic chamber and axotomized within the axonal compartment (**Fig. 1b**), there was no loss in viability post-axotomy (**Supplementary Fig. 1**), similar to *in vivo* findings [19], and injured axons regrew [11, 16]. Supporting the use of this approach, we previously found that axotomy performed within the microfluidic chambers induced rapid expression of the immediate early gene *c-fos* [11], as reported *in vivo* [20]. Neurons labeled with retrograde tracer, Alexa 568-conjugated cholera toxin, also showed a significant decrease in Nissl staining in the somata reflective of chromatolysis at 24 h post-axotomy [21]

(**Supplementary Fig. 1**). Together, this model recapitulated key features of axotomy *in vivo*.

Spine density decreases after distal axon injury

Decreased spine density is seen *in vivo* in models of traumatic brain injury and spinal cord injury [22, 23]. To determine whether similar structural changes occur in cultured pyramidal neurons following distal axotomy, we quantified spine density within the somatodendritic compartment of axotomized neurons that were retrogradely labeled using mCherry rabies virus. Spine density significantly declined 24 h and 48 h post-axotomy compared to before axotomy (**Fig. 1c,d**). In contrast, uninjured control neurons showed increased spine density as expected to occur during normal maturation (**Fig. 1c,d)**.

We next analyzed specific spine types that were lost. We found a preferential loss in the density of thin and stubby spines at both 24 h and 48 h post-axotomy compared to pre-axotomy (**Fig. 2a**). The density of mushroom spines remained stable at both 24 h and 48h after axotomy, unlike in the uninjured control neurons where spine density of all spine types increased. The reduction in spine density following axotomy suggests that either dendritic spines were being eliminated or, conversely, that there was a reduction in new spine formation following axotomy. Further analysis of our before and after axotomy images revealed that axotomy caused both a significant increase in the percentage of spines eliminated *and* a significant reduction in the percentage of new spines formed 24 h post-axotomy (**Fig. 2b-d**). Thus, axotomy affected both elimination and formation of spines to result in lower dendritic spine density.

Increased synaptic vesicle release rate follows axon injury

To further evaluate how synapses are modified following distal axon injury, we next investigated whether presynaptic release properties were altered at synapses onto injured neurons. To address this question, we retrogradely infected neurons using a modified eGFP rabies virus to label injured neurons and then used FM dyes to optically measure synaptic vesicle release onto these directly-injured neurons (**Fig. 3a)**. The use of FM dyes provided us with a non-selective, unbiased method to label a majority of presynaptic terminals within the somatodendritic compartment [24]. FM puncta highly colocalized with synapsin1 immunolabeling (93%), which is present at both inhibitory and excitatory terminals, validating our FM dye loading strategy (**Supplementary Fig. 2**). We examined the synaptic vesicle release rate of FM puncta that colocalized with axotomized eGFP expressing neurons. At 24 h post-axotomy, there was no change in synaptic vesicle release rate compared to eGFP expressing uninjured control samples (**Fig. 3b,c**). In contrast, 48 h after axotomy synaptic vesicle release rate was significantly enhanced (**Fig. 3c**). Further, the FM decay time constant, τ, which has been inversely correlated with release probability [25] was significantly reduced at 48 h post-axotomy (control: 124.8 s ± 5.487 versus axotomy: 78.65 s ± 3.922; $p<0.0001$). These results were similar to those obtained by examining the entire image field of FM puncta closest to the barrier region within the somatodendritic compartment where a large percentage of axotomized neurons reside (**Supplementary Fig. 3**). The difference in presynaptic release rate persisted, though modestly, at 4 d post-axotomy in these cultured neurons (control: 95.14 s ± 1.282 versus axotomy: 77.19 s ± 1.165; $p<0.0001$; **Supplementary**

153 **Fig. 3**). Together, these data suggest a delayed and persistent increase in synaptic vesicle
154 release rate that occured following dendritic spine loss.

155 Next, we performed two control experiments to determine (1) whether cortical
156 cultures, which have more neuron variaiblity than hippocampal cultures, would behave
157 similarly to hippocampal cultures used in our experimental model, and (2) whether
158 axotomy of axons forming synapses onto postsynaptic targets would yield similar effects
159 as axotomy of untargeted axons. First, we performed the FM unloading experiments with
160 cortical neurons harvested from embryonic rats and found that these cultures showed
161 similar changes in presynaptic release 48 h post-axotomy (**Supplementary Fig. 3**). To
162 address the second question, we added a small number of target neurons to the axonal
163 compartment during cell plating. We previously demonstrated that synapses form
164 between two neuron populations plated into opposing compartments [12]. Axotomy of this
165 targeted population of neurons resulted in similar changes in presynaptic release rate as
166 axotomy of untargeted axons (**Supplementary Fig. 3**).

167 Dendritic spine density is lower following injury, suggesting fewer synapses,
168 thus, we next wondered whether the balance of responsive to unresponsive presynaptic
169 terminals might be altered following axotomy to account for the enhancement in
170 excitability. We measured the proportion of FM puncta that unloaded (responsive) or did
171 not unload (unresponsive) in response to field stimulation using extracellular electrodes [24]
172 (**Fig. 3d**). At 24 h post-axotomy when spine density was decreased, we observed no
173 change in the fraction of responsive and unresponsive FM puncta compared to uninjured
174 controls (**Fig. 3d**). However at 48 h post-axotomy, a significantly larger proportion of
175 puncta were responsive compared to puncta within uninjured control chambers (**Fig. 3d**).

Further, at 48 h post-axotomy we found an overall decrease in the number of loaded FM puncta (**Fig. 3e**). Together, our data suggest that distal axon injury leads to an overall decrease in synapses, including the number of presynaptic terminals, but that the smaller number of presynaptic terminals is more responsive to stimulation.

Enhanced glutamate release at synapses onto injured neurons

Our results support that distal axotomy triggers a retrograde and trans-synaptic cascade of events leading to enhanced neurotransmitter release rate. To confirm this, we performed electrophysiological recordings of AMPAR-mediated miniature excitatory postsynaptic currents (mEPSCs) from axotomized neurons 48 h post-axotomy and their age-matched uninjured controls. Biocytin was used to fill neurons following each recording to determine whether neurons extended axons into the axonal compartment and were axotomized. Axotomized neurons had a significant increase in mEPSC frequency, confirming our FM data and supporting an increased rate of presynaptic glutamate release (**Fig. 3f,g**). Membrane properties were equivalent between axotomized and uninjured control neurons, demonstrating that the health of these axotomized neurons was not substantially compromised (**Supplementary Table 1**). We observed a trend towards an increase in mEPSC amplitude following axotomy, however this effect was not significant (**Fig. 3g**).

We next wondered if the increased spontaneous release rate of glutamate was specific to directly injured neurons or more globally affected neighboring, uninjured neurons. To address this, we quantified mEPSC frequency between uncut and cut neurons within the same axotomized chamber. In recordings from directly injured neurons,

axotomy specifically increased mEPSC frequency. However, neighboring uninjured neurons that did not extend axons into the axonal compartment, did not have an increased mEPSC frequency (**Fig. 3h**). To further examine the effects of direct injury to axotomized neurons, we quantified FM release rate at nearby uninjured neurons that were not infected with the retrograde eGFP rabies virus. We found that the release rate was significantly decreased at these locations compared with synapses on directly axotomized neurons and not significantly different than at control uninjured neurons labeled with eGFP rabies virus (**Fig. 3i**). These observations confirmed that axotomy altered glutamatergic synaptic input onto injured neurons. Further, directly injured neurons trans-synaptically influenced presynaptic glutamate release without affecting nearby synapses at uninjured neurons.

SCI induces persistent and enhanced firing in layer Vb

To evaluate the *in vivo* relevance of our findings, we sought to determine whether distal injury of long projection neurons *in vivo* would preferentially induce enhanced excitability in these injured neurons. To do this, we wanted to use an *in vivo* model in which axonal damage occurs far from somata to minimize other effects of injury (e.g., inflammation, metabolic changes). We used a rat SCI model described previously [26] in which animals were subjected to a spinal cord contusion injury at thoracic level T9-10, and recording electrodes were implanted into the neurophysiologically-identified hindlimb motor cortex in ketamine-anesthetized animals. Electrode sites on single-shank microelectrode arrays (Neuronexus, Ann Arbor, MI) extended through cortical layers V and VI, allowing simultaneous recording throughout these cortical layers. Effective injury

to the corticospinal neurons innervating hindlimb motor neuron pools in the spinal cord was confirmed by stimulating electrode sites and confirming loss of evoked hindlimb movement. At each cortical location, 5 minutes of neural data was collected for offline analysis. At the end of the procedure, neural spikes were discriminated using principle component analysis. We examined firing rates [27] within layers Va, Vb, and VI between 4 weeks and 18 weeks post-SCI and compared the data to sham control animals. We found that the firing rate within layer Vb was significantly increased after SCI compared to sham controls (**Fig. 4**). Layer Vb contains the highest density of corticospinal somata, with estimates of nearly 80% of large pyramidal cells [28]. Also, after spinal cord injury, chromatolytic changes occur preferentially in layer Vb [29]. In layers Va and VI, which have few (layer Va) or no (layer VI) corticospinal neurons, we found that firing rates were not statistically different between SCI animals and sham controls. Together, these data confirm a persistent increase in spontaneous firing rates in remotely injured corticospinal neurons, and support the relevance of our *in vitro* model system.

Axotomy eliminates GABAergic terminals onto injured neurons

Loss of inhibition following distal injury contributes to enhance excitability *in vivo*, thus we wanted to test whether axotomy in our culture system results in a similar loss of inhibitory terminals. We performed retrospective immunostaining to determine the fraction of vGLUT1 or GAD67-positive FM puncta at 48 h post-axotomy (**Fig. 5a,b**). We found that axotomy did not alter the fraction of glutamatergic terminals, but significantly diminished the fraction of GAD67-positive puncta within the somatodendritic compartment. Further, we examined the fraction of vGLUT1 or vGAT

puncta colocalized with axotomized neurons labeled with an eGFP rabies virus (**Fig. 5c**). These results confirmed the preferential absence of inhibitory terminals following axotomy while the fraction of vGLUT1 puncta remained equivalent to uninjured control neurons.

To determine whether inhibitory synapses were functionally altered following axotomy, we recorded miniature inhibitory postsynaptic currents (mIPSCs) from axotomized and uninjured chambers 48h post-axotomy (**Fig. 5d-f**). We found that mIPSCs were more frequent in axotomized cultures compared with uninjured neurons, suggesting that while there are fewer inhibitory terminals, the remaining terminals have an increased rate of spontaneous GABA release. We next asked whether this change in inhibitory synapse function was restricted to directly injured neurons. Within the axotomized cultures, we compared both cut and uncut neurons and found that the mIPSC frequency was increased in both groups, but was not different between the directly axotomized neurons and their uncut neighbors. This suggests that the alteration of inhibitory synaptic transmission following axotomy affects both directly injured and neighboring, uninjured neurons.

Although the majority of GABAergic synapses are found on dendritic shafts or cell bodies, a minor population is also found on dendritic spines [30, 31] (**Supplementary Fig. 4**). Inhibitory synapses formed on dendritic spines allow for compartmentalization of dendritic calcium levels involved in regulation of neuronal activity [32, 33]. To investigate whether dendritic spines receiving inhibitory inputs (i.e., inhibited spines) are lost following axotomy, we quantified the number of inhibitory and excitatory presynaptic terminals onto spines of cultured pyramidal neurons using retrospective immunostaining

for inhibitory (vGAT) and excitatory (vGLUT1) synapse markers. We found a significant decrease in the fraction of vGAT-positive spines at 48h post-axotomy compared to uninjured control (**Fig. 5g-i)** with no significant influence on glutamatergic spines. Together, our data suggest that axotomy caused a preferential loss of inhibitory terminals onto axotomized neurons, including inhibitory terminals formed onto dendritic spines, and that increased spontaneous GABAergic transmission might compensate to some degree for these lost terminals.

Local activity and transcription regulate remodeling

Efficient axon regeneration requires signaling from the site of injury to the nucleus in multiple model systems [6], yet the signaling events required for synaptic remodeling following distal axotomy remain unclear. Breach of the axonal membrane following axon injury causes an influx of calcium and sodium ions into the intra-axonal space, potentially influencing signaling to the nucleus and gene expression. To determine whether local influx of sodium and calcium ions at the time of injury is required for axotomy-induced spine loss, we performed axotomy within the axonal compartment in which axons were treated with a local activity blockade during axotomy. This local activity blockade solution (ABS) included low-Ca^{2+}, high-Mg^{2+}, and TTX (0.5 mM $CaCl_2$, 10 mM $MgCl_2$, 1 µM TTX) to prevent influx of sodium and reduce calcium influx. This local activity blockade was applied solely to the axonal compartment for 1 h during axotomy. We labeled neurons extending axons into the axonal compartment using a retrograde eGFP rabies virus and quantified spine density before and 24 h following axotomy and compared these measurements to cultures with vehicle applied to axons

during axotomy (**Fig. 6a,b**). Strikingly, we found that local activity blockade at the injury site prevented axotomy-induced spine loss. These data suggest that local activity instructs retrograde signaling and spine loss.

To determine whether injury-induced transcription is required for these trans-synaptic changes, we treated the somatodendritic compartment with the reversible transcriptional blocker DRB 15 min prior to axon injury and removed the drug 45 minutes later. We found that blocking transcription during this brief time was sufficient to prevent axotomy-induced spine loss 24 h post-axotomy compared with similarly treated uninjured control chambers (**Fig. 6c**). Further, DRB treatment at the time of injury prevented significant changes in the proportion of responsive FM puncta (**Fig. 6d**) and in synaptic vesicle release rate 48 h post-axotomy (**Fig. 6e**). However, action potential blockade with TTX in the somatodendritic compartment for ~1 h at the time of injury did not affect injury-induced changes in presynaptic release or the proportion of responsive puncta 48 h after axotomy (**Fig. 6f,g**). Further, application of HBS or DMSO as respective vehicle controls to TTX or DRB treatments did not alter injury-induced increase in presynaptic release. We conclude that both local activity at the site of injury and a transcriptional response were critical mediators of the delayed trans-synaptic changes in presynaptic release properties following distal axon injury.

Differential gene expression at 24 h post-axotomy

Our data show that a transcriptional response was required immediately after axotomy to induce retrograde changes in synaptic vesicle release onto injured neurons. To identify genes that might mediate this process within a longer therapeutically-relevant

time window, we performed a gene expression study to identify differentially expressed transcripts within the somatodendritic compartment at 24 h post-axotomy compared to uninjured controls (**Supplementary Fig. 5**). We found 615 transcripts that were significantly changed following injury (one-way between-subject ANOVA, $p < 0.05$) (**Fig. 7a; Supplementary Table 2**). Confirming that the transcription response *in vitro* recapitulated *in vivo* findings, we found Jun upregulated 1.41 fold in our microfluidic cultures 24 h post-axotomy [19].

Netrin-1 mRNA down-regulated post-axotomy

Next we sought to identify potential trans-synaptic mediators that may influence synaptic vesicle release at synapses onto injured neurons. We focused on differentially expressed transcripts that are known to localize to cell-cell contacts, such as synapses (**Supplementary Table 3**). We identified netrin-1 (*Ntn1*) as significantly downregulated 24 h following axotomy, consistent with published findings that netrin family proteins are downregulated following injury in adult rats [34] (**Fig. 7b**). Netrin-1 is a secreted axon guidance and synaptogenic cue that is enriched at mature dendritic spines [35] where it induces clustering of its receptor, DCC, and enhances synapse maturation [36]. To confirm that *Ntn1* expression is downregulated following nerve injury *in vivo*, we analyzed microarray data from a previously published study which examined cortical gene expression from retrograde labeled layer V cortex of young adult rats (2 months) subjected to either sham injury or spinal cord hemisection at thoracic level 8 [37] (**Fig. 7c**). Our analysis of this raw data confirmed that spinal cord injury significantly reduced netrin-1 expression in cortical layer V by 7 days, consistent with our in vitro findings.

Together, the significant decrease in *Ntn1* expression both *in vitro* and *in vivo* suggests a reliable response induced by distal axonal damage.

Exogenous netrin-1 normalizes injury-induced changes

The downregulation of netrin-1 following injury led us to ask whether adding exogenous netrin-1 might rescue, to some degree, the axotomy-induced synaptic changes. To test this we applied exogenous netrin-1 to the somatodendritic compartment 40 h after axotomy and evaluated the resulting changes in spine density, synaptic vesicle responsiveness, and disinhibition. We performed live imaging of somatodendritic domains before and after axotomy to measure spine density changes and found that netrin-1 treatment for 8 h was sufficient to normalize spine density to pre-axotomy levels (**Fig. 8a,b**). We then used FM dyes to compare presynaptic release properties between axotomized and uninjured controls. Exogenous netrin-1 increased the total number of FM puncta at 48 h post-injury to levels found in uninjured controls and reduced the percentage of responsive puncta to levels found in uninjured controls (**Fig. 8c,d**). We next tested whether netrin-1 might rescue axotomy-induced disinhibition. Netrin-1 treatment following axotomy normalized the density of inhibitory terminals (vGAT labeled) at axotomized neuron without significantly altering the density of glutamatergic terminals (vGLUT1 labeled) (**Fig. 8e,f**).

Because DCC protein levels parallel netrin-1 expression changes [38, 39], we next confirmed that DCC levels were downregulated at synapses formed onto the somatodendritic domain of axotomized neurons (**Fig. 8g,h**). Local synaptic DCC immunofluorescence at spines of axotomized neurons were decreased at 48 h post-injury.

Further, application of exogenous netrin-1 normalized synaptic DCC levels to that similar to uninjured controls (**Fig. 8g,h**).

If downregulation of netrin-1 signaling regulates axotomy-induced synaptic remodeling, we would expect that blocking netrin-1 signaling in uninjured neurons would be sufficient to cause both reductions in spine density and the density of inhibitory terminals. Spine density in uninjured cultures treated with a DCC function blocking antibody for 24 h was significantly reduced after treatment compared to control chambers treated with an IgG antibody (**Fig. 8i**). Further, we found that blocking DCC was sufficient to cause a reduction in the density of vGAT puncta, but not vGLUT1 puncta, per eGFP-filled neuron area (**Fig. 8j**). Together, our data suggest that netrin-1 signaling may play a critical role in regulating synaptic remodeling following axonal damage, including in modulating inhibition following injury.

Discussion

While axon regeneration following injury is extensively studied, much less is known about how proximal neurons within the mammalian brain are affected following axonal damage [40] and more specifically how synapses onto injured neurons are remodeled. We used a model system to enable the study the cellular mechanisms of synaptic remodeling following axon injury; this model recapitulated several hallmarks of neurons subjected to axonal injury *in vivo*, including chromatolysis [6, 21], retrograde spine loss [4, 22, 23], retrograde hyper-excitability [1-3], and disinhibition [2, 9, 10]. Axotomy-induced transcriptional changes in this *in vitro* model are also consistent with *in vivo* findings [7, 20]. Because of the ability to separate neuronal compartments, this tool facilitates the

383 investigation of axotomy-induced retrograde signaling intrinsic to neurons and the
384 resulting effects to interneuronal communication.

385 Our results suggest that retrograde remodeling requires local signaling at the site
386 of injury mediated by sodium and/or calcium influx to activate a rapid transcriptional
387 response. Both post-synaptic dendritic spine loss and trans-synaptic changes in
388 presynaptic inputs required immediate transcription. Our data is consistent with axonal
389 injury signaling in other non-CNS model systems [6]. Localized reversal of a sodium
390 calcium exchanger (NCX) at the site of injury may amplify calcium influx and contribute
391 to long range signaling [41]. In peripheral neurons calcium waves can locally propagate to
392 the nucleus to induce a transcriptional response [42]. The localized influx of calcium may
393 be a priming effect for retrograde transport of signaling complexes required to initiate
394 transcription [6].

395 Our data showed that axotomy-induced spine loss was followed by a specific loss
396 of inhibitory inputs. Interestingly, specific loss of inhibitory, and not excitatory, terminals
397 suggests that preserved excitatory inputs may remain available for some period of time
398 following injury. Because of the spine loss, these excitatory inputs could form shaft
399 synapses or some may become orphan presynaptic sites following injury. Large headed
400 dendritic spines could also receive multiple excitatory inputs, stabilizing them, and
401 allowing them to find new partners over time. The increased spontaneous release of
402 glutamate at injured neurons 48 h following axotomy, without an increase in the number
403 of excitatory terminals, suggests that the maintained excitatory inputs may contribute to
404 the hyper-excitability post-injury.

405 The sequential post- and then pre- synaptic changes following axotomy suggest a
406 trans-synaptic mechanism. These post- and then pre- synaptic changes are consistent with
407 the involvement of synaptic homeostasis where retrograde molecules are released post-
408 synaptically to influence presynaptic release. Further support for the involvement of
409 trans-synaptic mechanisms comes from our observation of an increase in spontanenous
410 neurotransmitter release localized at excitatory synapses onto axotomized neurons, but
411 not at neighboring excitatory synapses onto uninjured neurons. The significantly
412 enhanced firing rate following SCI in cortical layer Vb, but not layers Va and VI,
413 provides additional support for this specificity. Interestingly, we also found an increase in
414 spontaneous release at inhibitory terminals, although fewer inhibitory terminals remain
415 following axotomy. The increase in GABA release rate may serve as compensation
416 mechanism for the axotomy-induced hyper-excitability.
417 Dendritic release of secreted proteins (e.g., BDNF, NT-3 and NT-4) and diffusible
418 molecules, such as nitric oxide, can trans-synaptically regulate neurotransmitter release
419 [43-45]. Injury of motoneuron projections to myocytes caused synaptic remodeling of inputs
420 to motoneurons which was influenced by nitric oxide synthesis [46]. While these previously
421 reported trans-synaptic signaling pathways were not detectably altered in our microarray
422 analysis, we did identify the secreted protein, netrin-1, as significantly downregulated in
423 our axotomized cultures 24 h post- axotomy. Downregulation of netrin-1 gene expression
424 was further confirmed *in vivo* through an analysis of independently acquired microarray
425 data. Netrin-1 is secreted locally from target cells and signals DCC receptors that are
426 present along axons [36] to influence presynaptic release and maturation [47, 48]. While
427 netrin-1 signaling is historically thought of in a developmental context, there is increasing

evidence of the importance of netrin-1 signaling in the adult CNS. Consistent with our *in vitro* findings, netrin family members are downregulated *in vivo* following spinal cord injury in adult rats [34, 49] and DCC remains persistently low after 7 months post-injury in adult rats [34]. Netrin-1 has also recently been tested as a potential therapeutic agent following injury and has been shown to improve recovery outcomes [50-52].

We found that adding exogenous netrin-1 one and a half days after axotomy dramatically increased spine density and the density of inhibitory terminals to levels found in uninjured controls. The restoration of inhibitory terminals in axotomized samples treated with netrin-1 is a novel and exciting finding. Evidence from C.elegans confirms a link between netrin-1 signaling and stabilization of $GABA_A$ receptors [53]. Yet, it remains unclear how netrin-1 signaling modulates inhibitory input and will be an important topic for future studies. In contrast to previous reports, we found that there was no reduction in the number of vGLUT1 positive terminals when blocking DCC [36], which could be explained by our shorter treatment times with DCC function blocking antibody.

Axonal damage within the CNS occurs in numerous disorders and diseases, but little is known about the overall impact on cortical circuit function. Importantly, our cell-based findings have broader applicability beyond spinal cord injury to numerous conditions where axonal damage is prevalent, such as other forms of traumatic brain injury, Alzheimer's disease, and multiple sclerosis. Further, remodeling is enhanced in embryonic or neonatal neurons, making the use of an *in vitro* approach using these neurons, together with *in vivo* models, advantageous for identifying pathways instrumental for neurological recovery [54].

Materials and Methods

Hippocampal cultures. Animal procedures were carried out in accordance with the University of North Carolina at Chapel hill Institutional Animal Care and Use Committee (IACUC). Dissociated hippocampal cultures were prepared from Sprague Dawley rat embryos (E18-E19) as previously described [11, 24] with the following modifications. Hippocampal tissue was dissected in dissociation media (DM) containing 82 mM Na_2SO_4, 30 mM K_2SO_4, 5.8 mM $MgCl_2$, 0.25 mM $CaCl_2$, 1 mM HEPES, 20 mM Glucose and 0.001% Phenol red. For enzymatic digestion, equal volumes of TrypLE Express (Invitrogen) and DM were added to the tissue and incubated at 37°C for 8 min. Tissue was then rinsed and gently triturated in neuronal culture media consisting of Neurobasal media (Invitrogen) supplemented with 1x B27 (Invitrogen), 1x Antibiotic-antimycotic (Invitrogen), 1x Glutamax (Invitrogen). Dissociated cells were resuspended in neuronal culture media to yield $12x10^6$ cells per ml.

Microfluidic chambers. Poly(dimethylsiloxane) (PDMS) microfluidic chambers were replica molded from microfabricated master molds as described previously [11]. All experiments used chambers with 900 µm long microgrooves to separate the somatodendritic and axonal compartments as described previously [11, 16, 24]. Microfluidic chambers were placed onto glass coverslips coated with 500-550 kDa Poly-D-Lysine (BD Biosciences). Approximately ~90,000 cells were plated into the somatodendritic compartment and axons extended into the adjacent axonal compartment after 5-7 days of culture. Axotomy was performed between 11 and 15 days in vitro (DIV) according to previously published procedures [11, 16]. Briefly, media was first removed from the axonal

compartment and stored for future use. The axonal compartment was then aspirated until completely devoid of fluid. The stored culture media was then returned immediately to the axonal compartment for the duration of the culture time. Microfluidic devices with equivalent viable cell populations were randomly chosen for either axotomy or uninjured control groups.

Retrograde labeling. Retrograde labeling was performed using either modified cholera toxin or rabies virus. Cholera Toxin Subunit B Alexa Fluor 488 or 568 (Life technologies, Molecular Probes; 1 µg in 200 µl of neuronal culture media) was added to the axonal compartment of the microfluidic chamber and incubated for ~ 15 h at 37°C. After 15 h of incubation, the axonal compartment media was removed, rinsed and replaced using fresh neuronal culture media before performing axotomy or imaging.

G-deleted Rabies-mCherry or eGFP virus [55] (Salk Institute; $1x10^5$ viral units) in 50 µl- conditioned media was added to the axonal compartment of each chamber and incubated for 2h at 37°C. Conditioned media was added back to the axonal compartments following two washes with fresh NBE media. Chambers were maintained in 37°C incubator for ~48 h until fluorescence expression was visible.

Cell viability assay. Dead cells were labeled using SYTOX Green (Invitrogen) at a final concentration of 1 µM and all cell nuclei were labeled with NucBlue Hoechst Stain (Invitrogen). Cells were incubated with SYTOX/Hoechst solution simultaneously in 1x PBS for 5 min at 37°C, washed with PBS, and fixed with 4% paraformaldehyde (PFA) in PBS containing 40 mg/ml sucrose, 1 µM $MgCl_2$ and 0.1 µM $CaCl_2$ for 15 min at room

497 temperature (RT). Coverslips were then rinsed three times with PBS and mounted onto
498 the glass slide using Fluoromount G (Southern Biotech). SYTOX positive ($Sytox^+$) cells
499 were manually counted in ImageJ using sum projected z-stack confocal images. Percent
500 cell viability is calculated using [(Hoechst - $Sytox^+$) / Hoechst] * 100.
501
502 *Nissl Staining.* Neuronal cultures retrogradely labeled with Cholera Toxin were
503 either axotomized or left uninjured. PDMS chambers were carefully lifted off from PDL
504 coated coverslips 24 h post-axotomy. Cultures on the coverslips were quickly rinsed
505 twice with PBS, fixed with 4% PFA for 30 min at RT, washed twice in PBS, and
506 incubated in 0.1% Triton X-100/PBS for 10 min at RT. Cultures were incubated for 20
507 min in NeuroTrace 500/525 Green Fluorescent Nissl Stain (1:100; Invitrogen) and
508 washed for 10 min in 0.1% Triton X-100/PBS. Cell nuclei were stained with DAPI
509 (Sigma-Aldrich), rinsed three times in PBS, and then the coverslip was mounted onto a
510 microscope slide using Fluoromount G.
511
512 *Immunocytochemistry.* PFA fixed neuronal cultures were permeabilized in 0.25%
513 Triton X-100 and blocked in 10% normal goat serum for 15 min each. Coverslips were
514 incubated with anti-MAP2 (1:1000; Millipore # AB5622), anti-beta tubulin III
515 (1:2000;Aves # TUJ), anti-GAD67 (1:2000; Aves labs # GAD), anti-vGLUT1 (1:100;
516 NeuroMab, clone N28/9, cat. # 75-066), anti-vGAT (1:1000; Synaptic Systems # 131
517 003), anti-DCC (1:100; Calbiochem # OP45), or anti-synapsin1 (1:500; Calbiochem #
518 574778) primary antibodies in 1% blocking solution for overnight at 4°C. Coverslips
519 were then incubated with goat anti-rabbit or goat anti-mouse or anti-chicken secondary

520 antibodies conjugated to Alexa-fluorophores (1:1000; Invitrogen) for 1h at RT.
521 Following PBS washes coverslips were mounted onto the glass slide.
522
523 *RNA isolation.* Total RNA from each of 3 axotomized chambers and 3 sham
524 manipulated chambers (6 total samples) was isolated from the somatodendritic
525 compartment of 14 DIV cultures, 24 h after manipulation. RNA was collected from the
526 entire somatodendritic compartment for our gene expression analysis; thus, a fraction of
527 neurons in the axotomized chambers were axotomized and the remaining fraction
528 uninjured or "uncut". RNA was isolated using an RNAqueous-Micro Kit (Ambion)
529 according to the manufactures instructions including DNase treatment, with
530 modifications specific to accessing the microfluidic compartment [16]. Briefly, 50 µl lysis
531 solution was added to one somatodendritic well and collected from the other
532 somatodendritic well after solution flowed through the somatodendritic compartment to
533 this adjacent well. Lysate was added to 50 µl of fresh lysis solution and mixed well by
534 careful pipetting. Further RNA purification steps were performed according to
535 the manufacturer's guidelines. Samples were maintained at -80^{o}C until prepared for
536 microarray gene expression.
537
538 *Microarray analysis.* Quantification of RNA integrity and concentration was
539 confirmed with an Agilent TapeStation 2200 at the UNC Lineberger Comprehensive
540 Cancer Center Genomics Core. Microarrays were processed at the UNC School of
541 Medicine Functional Genomics Core using the Affymetrix GeneChip WT Plus Reagent
542 Kit for cRNA amplification, cDNA synthesis, fragmenting and labeling. Samples were

hybridized to Rat Gene 2.0 ST Arrays (Affymetrix). Data analysis was performed with Affymetrix Expression Console software and Affymetrix Transcriptome Analysis Console v2.0 software to compare axotomized cultures to uninjured control samples using one-way between-subject ANOVA of RMA normalized intensities. Quality control data is presented in **Supplementary Fig. 5**. Because a fraction of the harvested cells were uninjured in our axotomized samples, we used modest fold change values for defining our list of significantly changed transcripts (fold change absolute value ≥ 1.1 and ANOVA p-value <0.05). To identify cell-cell adhesion transcripts we searched for the biological process gene ontology category 'cell-cell adhesion'. Fold change shown in **Fig. 7** was calculated by dividing the mean $\log_2$ intensity value of the uninjured control by the mean $\log_2$ intensity value of the axotomized culture samples.

Raw microarray data of cortical layers V/VI of female Wistar rats subjected to either spinal cord transections at thoracic layer 8 or sham injury 1 day and 7 days following injury was downloaded from EMBL-EBI Array Express (E-MTAB-794)[37]. Four animals were used for each condition and samples were hybridized to Rat Gene 1.0 ST Arrays (Affymerix). The microarray data was previously validated using qPCR. Data analysis was performed with Affymetrix Expression Console software and Affymetrix Transcriptome Analysis Console v2.0 software to compare cortical layers V/VI from lesioned to sham operated animals.

Image acquisition and dendritic spine analysis. High-resolution z-stack montages of mCherry or eGFP labeled live neurons were captured using either a Zeiss LSM 780 (63x 1.4 NA or 40x 1.4 NA oil immersion objective) or an Olympus IX81 microscope

(60x 1.3 NA silicon oil immersion objective). For live imaging, we captured "0 h" or "before axotomy" confocal z-stack images to create montages of neurons extending axons into the axonal compartment. Axotomy was performed on the same day after acquiring these images. Images were acquired from the same neuron 24 h post-axotomy. In some cases, images were also acquired from the same neurons at 48 h post-axotomy (**Fig. 1, 2 and 8**). Calibrated z-stack montages were analyzed for all dendrite and spine parameters. Primary dendrites were traced using the semiautomatic neurite tracing tool, Neuron J [56, 57]. The number of spines on all primary dendrites of each neuron were manually labeled and categorized as thin, stubby or mushroom shaped using Neuron Studio [58]. Spine density was calculated for 10 µm length of dendrite as [(# of spines / dendrite length)*10]. Blinded data analysis was perfomed.

FM dye experiments and analysis. Cultures in microfluidic chambers at 24 h (14 DIV), 48 h (15 DIV), and 4d (17 DIV) post-axotomy were loaded with lipophilic dye FM 5-95 (Invitrogen) using KCl mediated depolarization as described previously [24]. Briefly, cultures were first incubated for 30 min with pre-warmed HEPES-buffered solution (HBS; 119 mM NaCl, 5 mM KCl, 2 mM $CaCl_2$, 2 mM $MgCl_2$, 30 mM glucose, 10 mM HEPES). Media was then replaced with FM dye loading solution containing 10 µM FM 5-95, 20 µM AMPAR antagonist 6-cyano-7-nitroquinoxaline-2,3-dione disodium (CNQX; Tocris), 50 µM NMDAR antagonist D-(-)-2-amino-5-phosphonopentanoic acid (D-AP5; Tocris) in 90 mM KCl HBS for 1 min. The loading solution was replaced with HBS containing 10 µM FM 5-95 for 1 min and later rinsed

three times with a high-Mg^{2+}, low-Ca^{2+} solution (106 mM NaCl, 5 mM KCl, 0.5 mM $CaCl_2$, 10 mM $MgCl_2$, 30 mM glucose, 10 mM HEPES) containing 1 mM Advasep-7 (Biotium) to remove extracellular membrane-bound FM. Finally, cultures were washed in HBS containing 20 µM CNQX and 50 µM D-AP5 for at least three times, 1 min each. Next, we stimulated the microfluidic chambers using extracellular electrodes by placing a positive and negative electrode in each well of the somatodendritic compartment.

Electrical stimulation was provided by an AD Instrument 2 Channel Stimulus Generator (STG4002) in current mode with an asymmetric waveform (-480 µA for 1 ms and +1600 µA for 0.3 ms) for ~ 1 min at 20 hz for 600 pulses. The FM 5-95 imaging was performed as described previously using a spinning disk confocal imaging system [24]. Z-stacks (31 slices) were captured every 15 s during the baseline (1 min), stimulation (1 min), and after stimulation (2 min) periods. This stimulation pattern was optimized for efficient FM unloading within these microfluidic chambers and the frequency is greater than typically used in open well dishes. At least 3 baseline images were acquired before electrical stimulation.

Blinded data analysis was perfomed. Sum projected confocal z-stack were converted to 8-bit images and registered using TurboReg, an Image J plugin. We background subtracted the image stack using the image 3 min after stimulation began. Image stacks were thresholded to a pixel value of 15. FM puncta between 0.4 to 10 μm^2 were analyzed. We measured the intensity of each punctum in the whole field or specifically on eGFP labeled neurons (**Fig. 3a-c**) throughout all time-series. To analyze the unloading kinetics of FM puncta on eGFP labeled neurons, we first thresholded the eGFP image and then created an outline enclosing all the eGFP labeled regions including

spines. The outlined ROI was superimposed on the FM labeled image and the intensity of each punctum in the selected ROI (eGFP outline) was measured throughout all time series. We normalized fluorescence intensity of each puncta to the frame before stimulation. Puncta with >5% unloading after 1 min were used in the analysis as unloaded puncta. Time constants were estimated by curve fitting unloading kinetics to a single exponential decay function [24]. Curve fitting was done in MATLAB and FM puncta with time constants longer than 3 min were excluded from the analysis and assumed to be non-releasing. Number of FM puncta that unload >5% after 60s were classified as responsive using image stacks that were not background subtracted; puncta that did not meet this criteria were classified as unresponsive.

In activity and transcription blocking experiments, the FM 5-95 unloading experiment was performed as mentioned above at 48 h post-axotomy. The intensity measurements of each punctum in the whole field and subsequent analysis of FM unloading kinetics was performed as mentioned above.

To determine the fraction of vGLUT1 or GAD67-positive FM puncta, the somal compartment of 15DIV cultures were loaded with FM 4-64FX (10 μM; Invitrogen), fixable analog of FM 4-64 membrane stain, using KCl mediated depolarization as described above. Following subsequent strip and wash steps, cells were fixed with 4% PFA in PBS and immunostained with anti-GAD67 and anti-vGLUT1 antibodies. Total number of vGLUT1, GAD67, and FM puncta were acquired by processing confocal Z-stack images using 3D foci picker, an ImageJ plugin [59].

635 *Drug treatments.* Local activity blockade solution (ABS), which includes low-
636 Ca^{2+}, high-Mg^{2+}, and TTX (0.5 mM $CaCl_2$, 10 mM $MgCl_2$, 1 μM TTX) was applied soley
637 to the axonal compartment for 1 h during axotomy (15 min prior and 45 min after
638 axotomy). 5,6-dichloro-1-β-D-ribofuranosyl-1H-benzimidazole (DRB; Sigma-Aldrich #
639 D1916) was suspended in DMSO and applied to the somatodendritic compartment at a
640 final concentration of 80 μM for 1 h during axotomy (beginning 15 min prior to
641 axotomy). Tetrodotoxin citrate (TTX; Tocris Bioscience # 1078) was suspended in HBS
642 and applied to the somatodendritic compartment at a final concentration of 1 μM for 1 h
643 during axotomy (beginning 15 min prior to axotomy). Media stored from the axonal
644 compartment prior to treatment was added back to the axonal compartment after
645 treatment. Exogenous netrin-1 was applied to the somatodendritic compartment 1 $^1/_2$ days
646 after axotomy, when spine changes were observed, at a final concentration of 625 ng/ml.
647 A similar netrin-1 concentration has been used for cortical neurons over a treatment time
648 of 1-2 days to examine netrin-specific responses [60]. Netrin-1 was applied for 8-10 h to
649 observe stable synaptic changes. For DCC function blocking experiments, anti-DCC
650 (mDCC; Calbiochem # OP45) and isotype control (mIgG; BD pharmingen #554121) was
651 applied to the somatodendritic compartment of uninjured chambers at a final
652 concentration of 1 μg/ml for 24 h.
653
654 *Microscopy.* FM and fixed imaging was performed using CSU-X1 (Yokogawa)
655 spinning disk confocal imaging unit configured for an Olympus IX81 microscope (Andor
656 Revolution XD). Live imaging of neurons for spine analysis was captured using a Zeiss
657 LSM 780 confocal microscope with a Plan-Apochromat 40x objective (NA 1.4) at the

658 UNC Neuroscience microscopy core facility. Excitation for the spinning disk confocal
659 imaging system was provided by 405 nm, 488 nm, 561 nm, and/or 640 nm lasers. The
660 following bandpass emission filters (BrightLine, Semrock) were used: 447/60 nm
661 (TRF447-060), 525/30 nm (TRF525-030), 607/36 nm (TR-F607-036), 685/40 nm (TR-
662 F685-040). For FM imaging, the spinning disk confocal imaging system was used with
663 excitation at 561 nm and the 685/40 nm emission filter. We used 2x2 binning to reduce
664 the laser intensity and acquisition time for each frame; each z-stack was obtained in ~5 s.
665 For the Zeiss LSM 780, signal was acquired from eGFP (493 nm - 558 nm), Alexa 568
666 (569 nm - 630 nm), and Alexa 647 (640 nm - 746 nm).
667
668 *Whole-Cell Electrophysiology.* For whole-cell recordings, neurons were visually
669 identified with infrared differential interference contrast optics. Cells were recorded in
670 voltage-clamp configuration with a patch clamp amplifier (Multiclamp 700A), and data
671 were acquired and analyzed using pCLAMP 10 software (Molecular Devices). Patch
672 pipettes were pulled from thick-walled borosilicate glass with open tip resistances of 2–7
673 MΩ. Series and input resistances were monitored throughout the experiments by
674 measuring the response to a −5-mV step at the beginning of each sweep. Series
675 resistance was calculated using the capacitive transient at the onset of the step and input
676 resistance was calculated from the steady-state current during the step. Recordings were
677 sampled at 10 kHz and bessel filtered at 2 kHz. No series resistance compensation was
678 applied.
679 Prior to recording, microfluidic chambers and PDMS molds were removed and
680 the glass coverslips containing cells were mounted onto a submersion chamber,

maintained at 32º C. Cultures were perfused at 2 mL/min with artificial cerebrospinal fluid (ACSF) containing 124 mM NaCl, 3 mM KCl, 1.25 mM Na_2PO_4, 26 mM $NaHCO_3$, 1 mM $MgCl_2$, 2 mM $CaCl_2$ and 20 mM d-(+)-glucose, saturated with 95% O_2, 5% CO_2. To determine if recorded neurons' axons entered the microfluidic chamber, 0.035 mM Alexa-594 was included in all internal solutions to allow for post-hoc visualization of neuronal morphology.

Events with a rapid rise time and exponential decay were identified as mEPSCs or mIPSCs respectively using an automatic detection template in pCLAMP 10, based on previously published methods[61]. mEPSC events were post-hoc filtered to only include events with a peak amplitude ≥5 pA and a ≤3 ms 10-90% rise time. Mean mEPSC parameters were quantified from a 10 min recording period and mIPSC parameters were sampled from a 5 min recording period. Neurons were excluded from analysis if R_{series} was >25 MΩ anytime during the recording.

mEPSCs Recordings. mEPSC recordings were performed similar to previously described[62]. AMPAR-mediated mEPSCs were isolated by voltage-clamping neurons at -70 mV and by supplementing the ACSF with TTX citrate (1 μM, Abcam), the GABA (A) receptor antagonist picrotoxin (50 μM, Sigma-aldrich), and the NMDA receptor antagonist D, L-2-amino-5 phosphonopentanoic acid (100 μM, AP5, Abcam). The internal solution contained: 100 mM $CsCH_3SO_3$, 15 mM CsCl, 2.5 mM $MgCl_2$, 5 mM QX-314-Cl, 5 mM tetra-Cs-BAPTA, 10 mM HEPES, 4 mM Mg-ATP, 0.3 mM Na-GTP, and 0.5% (w/v) neurobiotin with pH adjusted to 7.25 with 1 M CsOH and osmolarity adjusted to ~295 mOsm with sucrose.

704

705 *mIPSC recordings.* mIPSCs were isolated by supplementing the ACSF with TTX
706 citrate (1 μM), the NMDA receptor antagonist AP5 (100 μM), and the AMPA/Kainate
707 receptor antagonist 6,7-dinitroquinoxaline-2,3-dione (20 μM, DNQX, dissolved in
708 DMSO for a final concentration of 1% v/v DMSO in ACSF, Abcam). For mIPSC
709 recordings, the pipette solution contained a relatively lower chloride concentration,
710 similar to intracellular chloride concentrations that are present in more mature neurons [63].
711 This pipette solution contained, 110 mM $CsCH_3SO_3$, 2.5 mM $MgCl_2$, 5 mM QX-314-Cl,
712 5 mM tetra-Cs-BAPTA, 10 mM HEPES, 4 mM Mg-ATP, 0.3 mM Na-GTP, and 0.5%
713 (w/v) neurobiotin with pH adjusted to 7.28 with 1 M CsOH and a 300 mOsm osmolarity.
714 Following break-in, neurons were first voltage-clamped at -70 mV for at least three
715 minutes to allow dialysis with pipette solution, after which the voltage was gradually
716 changed to 0 mV, where it was maintained for duration of the recording.

717

718 *SCI injury and in vivo electrophysiology.* Nineteen adult male, Fischer-344 inbred
719 rats (Harlan Laboratories, Indianapolis, IN) were selected for this study. A total of 14 rats
720 received a contusion injury in the thoracic cord at level T9–T10, whereas 5 rats were
721 randomly selected as uninjured controls. After a minimum of 4 weeks following SCI,
722 intracortical microstimulation (ICMS) and single-unit recording techniques were used in
723 the hindlimb motor area (HLA) to determine movements evoked by ICMS and spike
724 rates. The protocol was approved by the University of Kansas Medical Center
725 Institutional Animal Care and Use Committee.

726 Spinal cord surgeries were performed under ketamine hydrochloride (80
727 mg/kg)/xylazine (7 mg/kg) anesthesia and aseptic conditions. Each of the SCI rats
728 underwent a T9–T10 laminectomy and contusion injury using an Infinite Horizon spinal
729 cord impactor (Precision Systems and Instrumentation, LLC, Fairfax Station, VA) with a
730 200 Kdyn impact. At the conclusion of surgery, 0.25% bupivacaine hydrochloride was
731 applied locally to the incision site. Buprenex (0.01mg/kg, SC) was injected immediately
732 after surgery and 1 day later. On the first week after surgery, the rats received daily
733 injections of 30,000U penicillin in 5mL saline. Bladders were expressed twice daily until
734 the animals recovered urinary reflexes.
735 Post-SCI surgical and neurophysiological procedures were conducted under
736 aseptic conditions 4 to 18 weeks post-SCI. At the time of these procedures, ages ranged
737 from 4.5 to 7.5 months. After an initial, stable anesthetic state was reached using
738 isoflurane anesthesia, isoflurane was withdrawn and the first dose of ketamine
739 hydrochloride (100 mg/kg)/xylazine (5 mg/kg) was administered. The rats were placed in
740 a Kopf small-animal stereotaxic instrument and a craniectomy was performed over the
741 motor cortex. The dura was incised and the opening filled with warm, medical grade,
742 sterile silicone oil. Core temperature was maintained within normal physiological limits
743 using a feedback-controlled heating pad during the entire procedure. A stable anesthetic
744 level was assessed by monitoring the respiratory and heart rate, and reflexes to noxious
745 stimuli.
746 In each rat, neuronal recordings were begun at ~3 h after initiation of the
747 procedure. Neuronal action potentials (single-units or spikes) were recorded with a
748 single-shank, 16-channel Michigan-style linear microelectrode probe (Neuronexus, Ann

749 Arbor, MI). A total of 15 channels were active in each procedure. The tip of the probe
750 was lowered to a depth of 1720 μm below the cortical surface, allowing accurate
751 determination of depth for each recording site. Because no hindlimb responses were
752 evoked using ICMS in SCI rats, the location of HLA in SCI rats was determined by the
753 stereotaxic coordinates derived in normal rats in a previous study (centered at 2 mm
754 posterior and 2.64 mm lateral to bregma). At each cortical location, electrical activity was
755 collected and digitized for 5 min from each of the 15 active sites using
756 neurophysiological recording and analysis equipment (Tucker Davis Technologies,
757 Alachua, FL). Neural spikes were discriminated using principle component analysis.
758 Sample waveforms (1.3 msec in duration) were collected that passed 5.5 X SD below
759 root mean square (RMS). After each experiment, the probe was cleaned with Opti-Free
760 solution (Alcon Laboratories, Fort Worth, TX), followed by ethanol and then rinsed
761 thoroughly in distilled water. The electrode impedance of each site remained at 0.9MΩ
762 for each experiment. At the end of the recording session, rats were humanely euthanized
763 with an overdose of sodium pentobarbital. Rats were randomized to SCI and control
764 groups. It was not possible to blind the surgeon performing the craniectomy and
765 neurophysiological data collection to group assignment, but these data were collected
766 using an automated system. The data analyst performing the post-hoc spike
767 discrimination procedures for each animal's neurophysiological data was blind to group
768 assignment.
769
770 *Statistics.* Statistics were analyzed using Graphpad Prism 6. For spine density
771 measurements, we used paired two-tailed t-tests. Sample sizes were determined by power

772 analysis, setting a desired Cohen's d statistical power to 0.8 and using a 5% error rate
773 (type I). For the paired spine density analyses (Fig. 1d, 6b-c, 8b, 8i), we calculated a
774 minimum sample size of 10 primary dendritic processes per condition using means and
775 standard deviations from Fig. 1d. For FM unloading analyses (Fig. 3c, 3i, 6e, 6g, suppl.
776 3b-f), we used a minimum sample size of 50 FM puncta per condition based on
777 previously published data[24] and using means and standard deviations from Fig. 3c. For
778 unresponsive/responsive FM puncta analyses (Fig. 3d-e, 6d, 6f, 8c-d), we calculated a
779 minimum sample size of 6 frames per condition using means and standard deviations of
780 unresponsive puncta in uninjured control versus 48h post-axotomy (Fig. 3e). For
781 vGAT/vGLUT1 puncta per area analyses (Fig. 5c, 8e-f, 8j), we calculated a minimum
782 sample size of 8 neuron fields per condition using the means and standard deviations of
783 vGAT puncta per area in control and axotomized samples (Fig. 5c). For the fraction of
784 GAD67 or vGLUT1 puncta to FM puncta analyses (Fig. 5a,b), we calculated a minimum
785 sample size of 18 frames per condition using the means and standard deviations found in
786 Fig. 5b. For DCC immunofluorescence per spine analyses (Fig. 8h), we calculated a
787 minimum of 75 samples per condition using the means and standard deviations of
788 controls and axotomized samples. We estimated requisite samples size for recordings of
789 spontaneous postsynaptic currents by assuming a doubling or halving of mEPSC or
790 mIPSC parameters following axotomy in correlation with the magnitude of changes
791 observed in our analysis of spine numbers, presynaptic release data, and based on similar
792 effect sizes being reported following synaptic activity blockade [64, 65]. Standard deviation
793 values for the power analysis were estimated based on previously published values from
794 dissociated hippocampal neuron electrophysiological recordings (Henry et al, 2012 and

795 Hartman et al, 2006). This analysis suggested we required 13 samples per group for
796 mEPSCs and 9 samples per group for mIPSCs. All recording, (Figures 3g-h, 5d-f) meet
797 or exceed the sample size required by our power analysis. For *in vivo* experiments,
798 hypotheses regarding spike firing rates were tested independently in each cortical layer
799 (Va, Vb and VI) using a two-tailed t-test, (alpha = 0.05). Samples were not excluded
800 from our data sets and sample size was determined based on our experience and previous
801 publications [24]. As confirmation of sufficient sample sizes, we used the means and
802 standard deviations for layer Vb control and SCI conditions and calculated a minimum of
803 112 samples for control and 282 samples for SCI conditions. For all experiments, sample
804 sizes were equal or greater than the calculated minimum sample sizes.

805

806 *Data availability.* The microarray data has been submitted to GEO (accession
807 number GSE89407). All relevant data will be available from authors upon request.

808

809 REFERENCES:

810 1. Nudo, R.J. *Front Hum Neurosci* **7**, 887 (2013).

811 2. Takechi, U., *et al. Clin Neurophysiol* **125**, 2055-2069 (2014).

812 3. Nudo, R.J. & Milliken, G.W. *J Neurophysiol* **75**, 2144-2149 (1996).

813 4. Oudega, M. & Perez, M.A. *J Physiol* **590**, 3647-3663 (2012).

814 5. Frost, S.B., *et al. J Neurophysiol* **89**, 3205-3214 (2003).

815 6. Rishal, I. & Fainzilber, M. *Nat Rev Neurosci* **15**, 32-42 (2014).

816 7. Urban, E.T., 3rd, *et al. Molecular and cellular biochemistry* **369**, 267-286 (2012).

817 8. Kim, B.G., *et al. Exp Neurol* **198**, 401-415 (2006).

818 9. Jacobs, K.M. & Donoghue, J.P. *Science* **251**, 944-947 (1991).

819 10. Ding, M.C., *et al. J Neurosci* **31**, 14085-14094 (2011).

820 11. Taylor, A.M., *et al. Nat Methods* **2**, 599-605 (2005).

821 12. Taylor, A.M., *et al. Neuron* **66**, 57-68 (2010).

822 13. Neto, E., *et al. The Journal of Neuroscience* **36**, 11573-11584 (2016).

823 14. Nakatomi, H., *et al. Cell* **110**, 429-441 (2002).

824 15. Will, B., *et al. Progress in Neurobiology* **72**, 167-182 (2004).

825 16. Taylor, A.M., *et al. J Neurosci* **29**, 4697-4707 (2009).

826 17. Banker, G.A. & Cowan, W.M. *Brain Res* **126**, 397-342 (1977).

827 18. Benson, D.L., *et al. J Neurocytol* **23**, 279-295 (1994).

828 19. Greer, J.E., *et al. J Neurosci* **32**, 6682-6687 (2012).

829 20. Ikeda, S. & Nakagawa, S. *Brain Res* **792**, 164-167 (1998).

830 21. McIlwain, D.L. & Hoke, V.B. *BMC Neurosci* **6**, 19 (2005).

831 22. Ghosh, A., *et al. Cereb Cortex* **22**, 1309-1317 (2012).

832 23. Gao, X., *et al. PLoS One* **6**, e24566 (2011).

833 24. Taylor, A.M., *et al. J Neurosci* **33**, 5584-5589 (2013).

834 25. Zakharenko, S.S., *et al. Nat Neurosci* **4**, 711-717 (2001).

835 26. Frost, S.B., *et al. J Neurotrauma* **32**, 1666-1673 (2015).

836 27. Lewicki, M.S. *Network* **9**, R53-78 (1998).

837 28. Nudo, R.J., *et al. The Journal of Comparative Neurology* **358**, 181-205 (1995).

838 29. Barron, K.D., *et al. J Neuropathol Exp Neurol* **47**, 62-74 (1988).

839 30. Chen, J.L., *et al. Neuron* **74**, 361-373 (2012).

840 31. Markram, H., *et al. Nat Rev Neurosci* **5**, 793-807 (2004).

841 32. Chiu, C.Q., *et al. Science* **340**, 759-762 (2013).

842 33. Higley, M.J. *Nat Rev Neurosci* **15**, 567-572 (2014).

843 34. Manitt, C., *et al. J Neurosci Res* **84**, 1808-1820 (2006).

844 35. Horn, K.E., *et al. Cell Rep* **3**, 173-185 (2013).

845 36. Goldman, J.S., *et al. J Neurosci* **33**, 17278-17289 (2013).

846 37. Jaerve, A., *et al. PLoS One* **7**, e49812 (2012).

847 38. Xu, K., *et al. Science* **344**, 1275-1279 (2014).

848 39. Manitt, C., *et al. J Neurosci* **29**, 11065-11077 (2009).

849 40. Canty, A.J., *et al. J Neurosci* **33**, 10374-10383 (2013).

850 41. Persson, A.K., *et al. J Neurosci* **33**, 19250-19261 (2013).

851 42. Cho, Y., *et al. Cell* **155**, 894-908 (2013).

852 43. Wong, Y.C. & Holzbaur, E.L. *J Neurosci* **34**, 1293-1305 (2014).

853 44. Branco, T., *et al. Neuron* **59**, 475-485 (2008).

854 45. Gonzalez-Forero, D. & Moreno-Lopez, B. *Neuroscience* **283**, 138-165 (2014).

855 46. Sunico, C.R., *et al. J Neurosci* **25**, 1448-1458 (2005).

856 47. Stavoe, A.K. & Colon-Ramos, D.A. *The Journal of Cell Biology* **197**, 75-88
857 (2012).

858 48. Colon-Ramos, D.A., *et al. Science* **318**, 103-106 (2007).

859 49. Ahn, K.J., *et al. Neurosci Lett* **419**, 43-48 (2007).

860 50. Lu, H., *et al. Front Med* **5**, 86-93 (2011).

861 51. Han, X., *et al. Mol Neurobiol* (2016).

862 52. Sun, H., *et al. Neurobiol Dis* **44**, 73-83 (2011).

863 53. Tu, H., *et al. Neuron* **86**, 1407-1419 (2015).

864 54. McKinley, P.A. & Smith, J.L. *J Neurosci* **10**, 1429-1443 (1990).

865 55. Wickersham, I.R., *et al. Neuron* **53**, 639-647 (2007).

866 56. Fu, M.M. & Holzbaur, E.L. *Autophagy* **10**, 2079-2081 (2014).

867 57. Nagendran, T. & Hardy, L.R. *Neuroscience* **199**, 548-562 (2011).

868 58. Rodriguez, A., *et al. PLoS One* **3**, e1997 (2008).

869 59. Du, G., *et al. Radiat Res* **176**, 706-715 (2011).

870 60. Menon, S., *et al. Dev Cell* **35**, 698-712 (2015).

871 61. Clements, J.D. & Bekkers, J.M. *Biophys J* **73**, 220-229 (1997).

872 62. Larsen, R.S., *et al. Neuron* **83**, 879-893 (2014).

873 63. Yamada, J., *et al. J Physiol* **557**, 829-841 (2004).

874 64. Hartman, K.N., *et al. Nat Neurosci* **9**, 642-649 (2006).

875 65. Henry, F.E., *et al. J Neurosci* **32**, 17128-17142 (2012).

876

Acknowledgements: We thank Stephanie Gupton for netrin-1, Kelly Carstens for preliminary gene expression work, Cassie Meeker for technical support, and Fabio Urbina for assistance in statistical analysis. We thank Richard Segal (MUSC), Julius Dewald (RIC) and Taylor lab members for their advice and discussions. **Funding:** A.M.T. acknowledges support from the Eunice Kennedy Shriver NICHD (K12 HD073945), NIMH (R42 MH097377), and an Alfred P. Sloan Research Fellowship. Imaging was supported by the Confocal and Multiphoton Imaging Core Facility of NINDS Center Grant P30 NS045892 and NICHD Center Grant (U54 HD079124). R.S.L was supported by NRSA predoctoral fellowship F31 MH091817 and the UNC Department of Cell Biology and Physiology's Dr. Susan Fellner fellowship. R.L.B. was supported in part by a grant from the National Institute of General Medical Sciences under award 5T32 GM007092. **Author contributions:** T.N. designed and performed experiments and wrote the manuscript. R.S.L. designed and performed electrophysiology experiments. R.L.B. designed and performed experiments.. S.B.F. performed experiments. B.D.P. designed experiments. R.J.N. designed and performed experiments. A.M.T. designed experiments and wrote the manuscript. **Competing financial interests:** Yes there is potential competing interest. A.M.T. is an inventor of the microfluidic chambers (US 7419822 B2) and has financial interest in Xona Microfluidics, LLC. T.N., R.L.B., R.S.L., R.J.N. and B.D.P. declare no competing financial interests.

Fig. 1: Distal axotomy of pyramidal neurons within microfluidic chambers induced dendritic spine loss on axotomized neurons. (**a**) 14 DIV rat hippocampal neurons cultured within a microfluidic chamber. Pyramidal neurons were retrogradely labeled using a G-deleted mCherry rabies virus added exclusively to the axonal compartment. (**b**) Cartoon illustration of *in vitro* axotomy (Axot.) within microfluidic chambers to selectively axotomize a subset of labeled neurons (red) that extend axons through the microgroove region. Axons of uninjured neurons (grey) extend axons within the somatodendritic compartment. (**c**) Representative images of mCherry-labeled neurons and dendritic segments (inverted fluorescence) from repeated live imaging of uninjured control (Uninj. cntl) and axotomized neurons. Axotomized neurons were imaged before axotomy on DIV 13 (before) and uninjured controls were also imaged on DIV 13 (0 h); both conditions were imaged at 14 DIV (24 h after). Image and inset scale bars, 50 and 5 µm, respectively. (**d**) Quantification of spine density illustrated in *(c)*. *Uninj. cntl*: n=20 dendrites; 5 neurons; 3 chambers over 3 experiments; #spines/TDL: 315/2698µm (0h), 388/2737µm (24h after). *Axot.*: n=26 dendrites; 5 neurons; #spines/TDL: 405/3569µm (before), 274/2998µm (24h after), 229/2821µm (48h after). 3 chambers over 3 experiments. Paired two-tailed t-test. **p<0.01, ****p<0.0001. Error bars, s.e.m.

Fig. 2: Axotomy causes dendritic spine loss and reduces new spine formation. (**a**) Quantification of stubby, mushroom, and thin spine densities before axotomy, 24h post-axotomy, 48h post-axotomy, and in uninjured controls. Uninjured controls and axotomized samples were imaged beginning at 13 DIV (labeled “0 h” or “Before”, respectively). *Uninj. cntl*: n=20 dendrites; 5 neurons; 3 chambers over 3 experiments;

#spines/TDL: 315/2698µm (0h), 388/2737µm (24h after). *Axot.*: n=26 dendrites; 5 neurons; #spines/TDL: 405/3569µm (before), 274/2998µm (24h after), 229/2821µm (48h after). 3 chambers over 3 experiments. Repeated-measure two-way ANOVA, Bonferroni post-hoc test. (**b**) Representative images of dendritic segments from uninjured control and axotomized neurons at 0 h or before axotomy, respectively, and 24 h after. Astericks indicate spines eliminated; arrows indicate formation of new spines. Scale bars, 5 µm. (**c-d**) Bar graphs represent percentage of spines eliminated (*c*) and newly formed (*d*) after 24h in controls and 24h post-axotomy. *Uninj. cntl*: n=28 dendrites; 6 neurons; #spines eliminated: 92; #spines formed: 177; TDL(0h, 24h after): 3147, 3148µm. *Axot*: n=35 dendrites; 6 neurons; #spines eliminated: 208; #spines formed: 75; TDL (before, 24h after): 4290, 3865µm. 3 chambers over 3 experiments. Unpaired two-tailed t-test. **p<0.01, ****p<0.0001. Error bars, s.e.m.

Fig. 3: Distal axotomy induces a delayed trans-synaptic increase in presynaptic-excitability onto axotomized neurons. (**a**) A representative neuron retrogradely labeled with a modified eGFP rabies virus via the axonal compartment. Enlarged region shows FM puncta colocalized with eGFP dendrites and spines (arrows). ImageJ 'fire' color look-up-table shown in *(b)*. Scale bar, 20 µm. (**b**) Representative images show FM puncta colocalized with eGFP dendrites (outlined in white dashed lines) before and after field stimulation in uninjured control, and 24h and 48h post-axotomy. Arrows highlight destaining at spines. Scale bars, 10 µm. (**c**) FM unloading of colocalized puncta 24h post-axotomy (control, n=185 puncta; axotomy, n=256 puncta) and 48h post-axotomy (control, n=232 puncta; axotomy, n=322 puncta). Two-way ANOVA, Bonferroni post-

hoc test. Inset shows FM decay time constant (τ) for puncta with τ<360sec (24h control, n=151; 24h axotomy, n=201; 48h control, n=211; 48h axotomy, n=304). (*b-c*) Unpaired two-tailed t-test. Each condition includes 5-6 chambers/neurons over 3 experiments. (**d**) Percent responsive and unresponsive FM puncta per neuron field (n=8 fields/chambers; 4 experiments). Unpaired two-tailed t-test, axotomy versus control for each timepoint. (**e**) Number of responsive and unresponsive FM puncta per frame at 48h post-axotomy (n=11 chambers; 5 experiments). Unpaired two-tailed t-test, unresponsive puncta. (**f**) Representative mEPSC traces 48h post-axotomy. (**g**) mEPSC frequency and amplitude at 48h post-axotomy (control, n=17 neurons; axotomy, n=20 neurons; 4 experiments). Inset: Cartoon depicts recordings from either uninjured control neurons (black) or directly injured neurons (red). (**h**) Analysis of mEPSC frequency and amplitude of cut neurons [cut (red), n=10 neurons] compared to neighboring uncut neurons within axotomized chambers [uncut (grey), n=10 neurons]. (*g-h*) Unpaired two-tailed t-test, Welch's correction. (**i**) FM unloading of neighboring uncut neurons identified by lack of eGFP (uncut neighbors, n=816 puncta), uninjured control neurons (uncut-labeled, n=232), and axotomized labeled neurons (cut-labeled, n=322). Two-way ANOVA, Bonferroni post-hoc test; Each condition, 5 chambers and 3 experiments. Decay time constant (τ) of FM puncta at 48h post-axotomy (uncut-labeled, n=211; cut-labeled, n=304; uncut neighbors unlabeled, n=703). One-way ANOVA, Bonferroni post-hoc test. * $p<0.05$, *** $p<0.001$. Error bars, s.e.m.

Fig. 4: Spinal cord injury increases spontaneous single-unit firing rate in layer Vb of hindlimb cortex 4-18 weeks following injury.

967 Mean spontaneous firing rates of isolated single-units in layers Va, Vb and VI of the
968 hindlimb motor cortex in control rats (n=5) and rats with a spinal cord contusion at T9-10
969 (n=14). Laminar estimates are based on the depths of electrode sites on a single-shank
970 multi-electrode array relative to the cortical surface [26]. In each rat, single-unit (spike)
971 activity was sampled from 4 to 6 locations within neurophysiologically-identified
972 hindlimb motor cortex. Data represent the mean firing rates of 1,744 isolated units in
973 Layers Va (control, n=124; SCI, n=312), Vb (control, n=155; SCI, n=390), and VI
974 (control, n=217; SCI, n=546). Two-tailed t-test, t=3.99, **** p<0.0001.
975
976 **Fig. 5: Distal axotomy induces culture-wide loss of inhibitory terminals and**
977 **increased frequency of spontaneous release events at GABAergic terminals.**
978 (**a**) Representative images of fixable FM4-64FX puncta (red) and vGLUT1 (green) co-
979 immunolabeling in uninjured chambers and 48h following axotomy. White circles
980 highlight vGLUT1 expression at FM-labeled terminals. Scale bars, 10 µm. Fraction of
981 vGLUT1+ FM puncta per neuron field at 48h post-axotomy normalized to uninjured
982 controls. n=18 neuron fields; 5 chambers over 3 experiments. (**b**) Fixable FM4-64FX
983 puncta (red) and GAD67 (green) co-immunolabeling. Quantification of GAD67-positive
984 FM puncta at 48h post-axotomy normalized to control. n=21 neuron fields; 5 chambers
985 over 3 experiments. (**c**) Number of vGLUT1 and vGAT puncta per neuron area
986 (axotomized or control) 48 h post-axotomy. n=8-9 neurons; 3 chambers per condition
987 over 3 experiments. (*a-c*) Unpaired two-tailed t-test. (**d**) Representative traces of mIPSC
988 recordings 48 h post-axotomy. (**e**) Quantification of mIPSC frequency and amplitude 48h
989 post-axotomy (control, n=9 neurons; axotomy, n=17 neurons). (mIPSC frequency:

unpaired two-tailed t-test with Welch's correction, p = 0.05; mIPSC amplitude: unpaired two-tailed t-test, p = 0.62). (**f**) Analysis of mIPSC frequency and amplitude from axotomized devices previously shown in (*e*) comparing neurons with axons that extended into the axonal compartment and were cut (cut, n=8 neurons), to neurons that did not extend axons into the compartment and were not cut (uncut, n=9 neurons). (mIPSC frequency: unpaired two-tailed t-test, p = 0.94; mIPSC amplitude: unpaired two-tailed t-test, p = 0.51). (*d-f*) Data shown were combined from 3 chambers. (**g**) Representative dendritic segments (retrogradely labeled with eGFP rabies virus) showing spines that are labeled with vGLUT1 (red) or vGAT (magenta) antibodies. White open circles highlight dendritic spines with vGLUT1 and/or vGAT synapses. (**h**) Fraction of vGLUT1- and vGAT-positive spines at 24h post-axotomy. n=12-14 neuron fields; 7 neurons per condition; #spines: 458 (uninj. cntl), 394 (axot.); 3 chambers over 3 experiments. (**i**) Fraction of vGLUT1- and vGAT- positive spines at 48 h post-axotomy. n=11-15 neuron fields; 8-9 neurons per condition; #spines: 460 (uninj. cntl), 413 (axot.); 3 chambers over 3 experiments. Scale bars, 5 µm. Unpaired two-tailed t-test. **p < 0.01, ***p < 0.001. Error bars, s.e.m.

Fig. 6: Injury-induced synaptic remodeling is triggered by retrograde propogation of injury signaling from axon-to-soma and gene transcription.

(**a**) Representative images of neurons within microfluidic chambers retrograde labeled with eGFP rabies virus (inverted grayscale) before and 24h post-axotomy with vehicle or local activity blockade solution (ABS) applied to axons for 1h during axotomy. Inset shows zoomed in dendritic regions. Image and inset scale bars, 50 and 5 µm,

respectively. (**b**) Quantification of before and after spine density data described in (*a*). *Axotomy (vehicle)*: n=29 dendrites; 5 neurons; 3 chambers over 3 experiments; #spines/TDL: 437/4185µm (before), 274/3868µm (after). *Axot. (ABS)*: n=33 dendrites; 5 neurons; 3 chambers over 3 experiments; #spines/TDL: 426/3889µm (before), 446/3700µm (after). (**c**) Quantification of spine density changes following application of transcription blocker (DRB) to the somatodendritic compartment for 1h during axotomy within microfluidic chambers. *DRB (uninj.)*: n=27 dendrites; 6 neurons; 3 chambers over 3 experiments; #spines/TDL: 362/4186µm (0h), 262/3934µm (24h after). *DRB (axot.)*: n=28; 6 neurons; 3 chambers over 3 experiments; #spines/TDL: 343/3414µm (before) 283/3248µm (after). (*b*,*c*) Unpaired two-tailed t-test, 24h post-axotomy (**d**) Percentage of responsive and unresponsive FM puncta at 48h post-axotomy. n=6 neuron fields/chambers per condition over 3 experiments. Unpaired two-tailed t-test, % responsive. (**e**) FM 5-95 unloading following 1h application of DRB during axotomy/control. *Uninj. DRB*: n=1580 puncta; 6 chambers per condition over 3 experiments. *Axot. DRB*: 2213 puncta; 6 chambers per condition over 3 experiments.(**f**) Percent of responsive and unresponsive puncta at 48h post-axotomy following application of TTX to the somatodendritic compartment for 1 h during injury. n=6 neuron fields/chambers per condition over 3 experiments. Unpaired two-tailed t-test, % responsive. (**g**) FM unloading curves following application of TTX.*Uninj. TTX*: n=1360 puncta; 6 chambers per condition over 3 experiments. *Axot. TTX*: n=1648 puncta; 6 chambers per condition over 3 experiments. Two-way ANOVA, Bonferroni post-hoc test. *p<0.05, **p<0.01, ***p<0.001, **** p<0.0001. Error bars, s.e.m.

Fig. 7: Netrin-1 gene expression is differentially regulated within the somatodendritic compartment following axotomy in microfluidic cultures and in vivo following spinal cord hemi-transection. Microarray analysis was performed on somatodendritic samples of uninjured controls and 24h post-axotomy cultures. Quality control data is presented in **Supplementary Fig. 5**. (**a**) Volcano plot showing differentially expressed RNAs that are significantly changed at 24h post-axotomy (One-way between-subject ANOVA; n=3 individual chambers each condition; **Supplementary Table 2**). (**b**) Microarray expression levels for *Ntn-1* within microfluidic chambers (left) and for housekeeping genes *Odc1* and *GAPDH (right)*. One-way between-subject ANOVA. (**c**) Microarray expression levels for *Ntn-1* (left) and *Odc1* and *GAPDH* (right) in cortical layers V/VI following hemi-transection at thoracic level 8. n=4 animals per group. *Ntn-1* levels are significantly reduced by 7 days following injury. Two-way ANOVA, Sidak's multiple comparisons test. *p<0.05. Error bars, s.e.m.

Fig. 8: Exogenous netrin-1 normalizes synaptic changes following distal axotomy. (**a**) Representative dendrites before and 48h post-axotomy treated with vehicle (HBS) or netrin-1 (Ntn1) beginning at 40h post-axotomy (inverted fluorescence). Arrows: new spines; red astericks: eliminated spines. Scale bars, 10 µm. (**b**) Quantification of spine density illustrated in (*a*). *Axotomy*: n=33 dendrites; 7 neurons; #spines/TDL: 392/3696µm (before), 263/3447µm (after). *Axotomy+netrin-1*: n=29 dendrites, 6 neurons; #spines/TDL: 293/3281µm (before), 363/3417µm (after). (**c**) Percent responsive FM puncta per neuron field at 48h post-axotomy with HBS or netrin-1. n=8-11 fields/chambers per condition over 5 experiments. (**d**) Number of responsive and

unresponsive FM puncta from (*c*). Significantly fewer unresponsive puncta followed axotomy compared to uninjured control (HBS). (**e-f**) Number of vGLUT1 and vGAT puncta per neuron area (uninjured control, axotomized+HBS, or axotomized+netrin-1) at 14 DIV. n=8-9 neurons; 3 chambers per condition over 3 experiments. (**g**) Representative DCC immunostaining (turquoise) in uninjured control, post-axotomy, and post-axotomy+netrin-1 in cultures with similar spine densities. Neurons were retrogradely labeled with fluorescent protein (FP, magenta) using an mCherry modified rabies virus. Scale bar, 10 µm. (**h**) Quantification of DCC immunofluorescence per spine region-of-interest (ROI). ROI: 2µm diameter circular region surrounding each spine. Control, n=295 ROIs; axotomy, n=293 ROIs; axotomy+Ntn1, n=210 ROIs. 8 neuron fields/3 chambers per condition; 3 experiments. (**i**) Quantification of spine density following 24h of control antibody (IgG ab.) or DCC function blocking antibody (DCC ab.). *IgG*: n=33 dendrites; 8 neurons; #spines/TDL: 464/4864µm (before), 419/4712µm (after). *DCC ab*: n=34 dendrites; 7 neurons; #spines/TDL: 404/4433µm (before), 222/3647µm (after). (**j**) Representative FP-labeled dendritic segments immunostained for vGAT (inverted) and vGLUT1 (inverted) following 24h application of IgG or DCC antibodies (outlined dendrites, solid magenta line). Neurons were fixed at 15-16 DIV, older than the cultures in (*e*,*f*). Scale bar, 10 µm. Quantification shown on the right. n=23 neuron fields per condition; 3 chambers per condition over 3 experiments. (*b*,*i*) Repeated-measure two-way ANOVA, Bonferroni post-hoc test; analyses included 1 chamber per condition for 3 experiments. (*c*,*j*) Unpaired two-tailed t-test. (*d-f*,*h*) One-way ANOVA, Bonferroni post-hoc test. Error bars, s.e.m. *p<0.05, ****p<0.0001

Supplementary Figures and Tables:

Supplementary Fig. 1: Distal axotomy of pyramidal neurons induces dissolution of Nissl substance without affecting cell viability.

Supplementary Fig. 2: FM puncta colocalize with synapsin1 immunolabeling.

Supplementary Fig. 3: FM unloading curves for (1) somatodendritic compartments, near the microgrooves of microfluidic chambers without retrograde labeling, and (2) cortical and targeted neuron populations subjected to axotomy.

Supplementary Fig. 4: Fluorescence micrograph of a dually innervated dendritic spine receiving both excitatory and inhibitory inputs.

Supplementary Fig. 5: RNA quality assessment and verification of microarray quality controls.

Supplementary Table 1: Membrane properties of uninjured controls vs. axotomized neurons 48 h post-axotomy

Supplementary Table 2: List of transcripts that were significantly changed 24 h after injury.

Supplementary Table 3: Cell-cell adhesion transcripts changed 24 h after injury ($p < 0.1$)

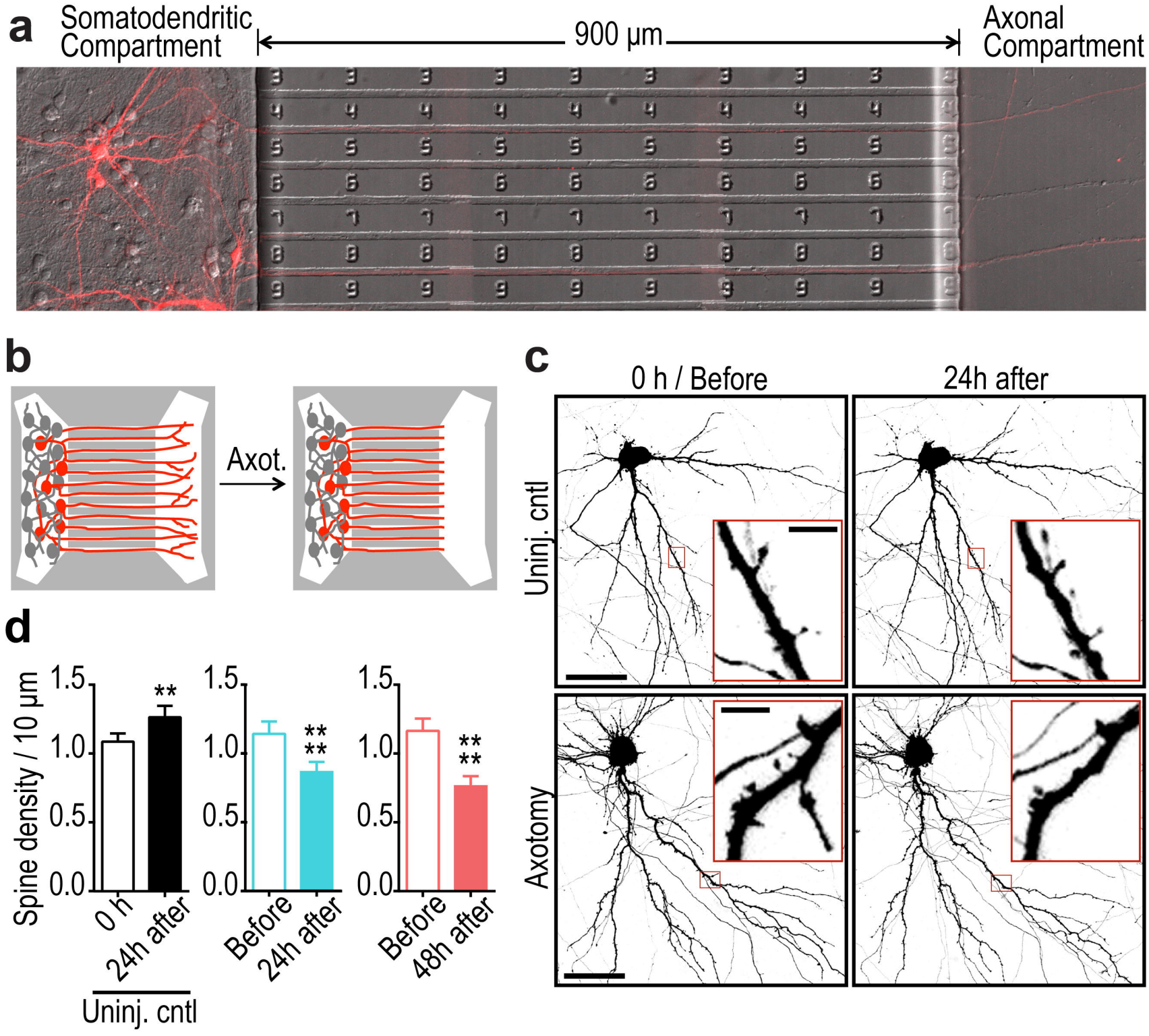
a
Somatodendritic Compartment
900 µm
Axonal Compartment
b
Axot.
c
0 h / Before
24h after
Uninj. cntl
Axotomy
d
Spine density / 10 µm
1.5
1.0
0.5
0.0
**
**
**
**
0 h
24h after
Before
24h after
Before
48h after
Uninj. cntl

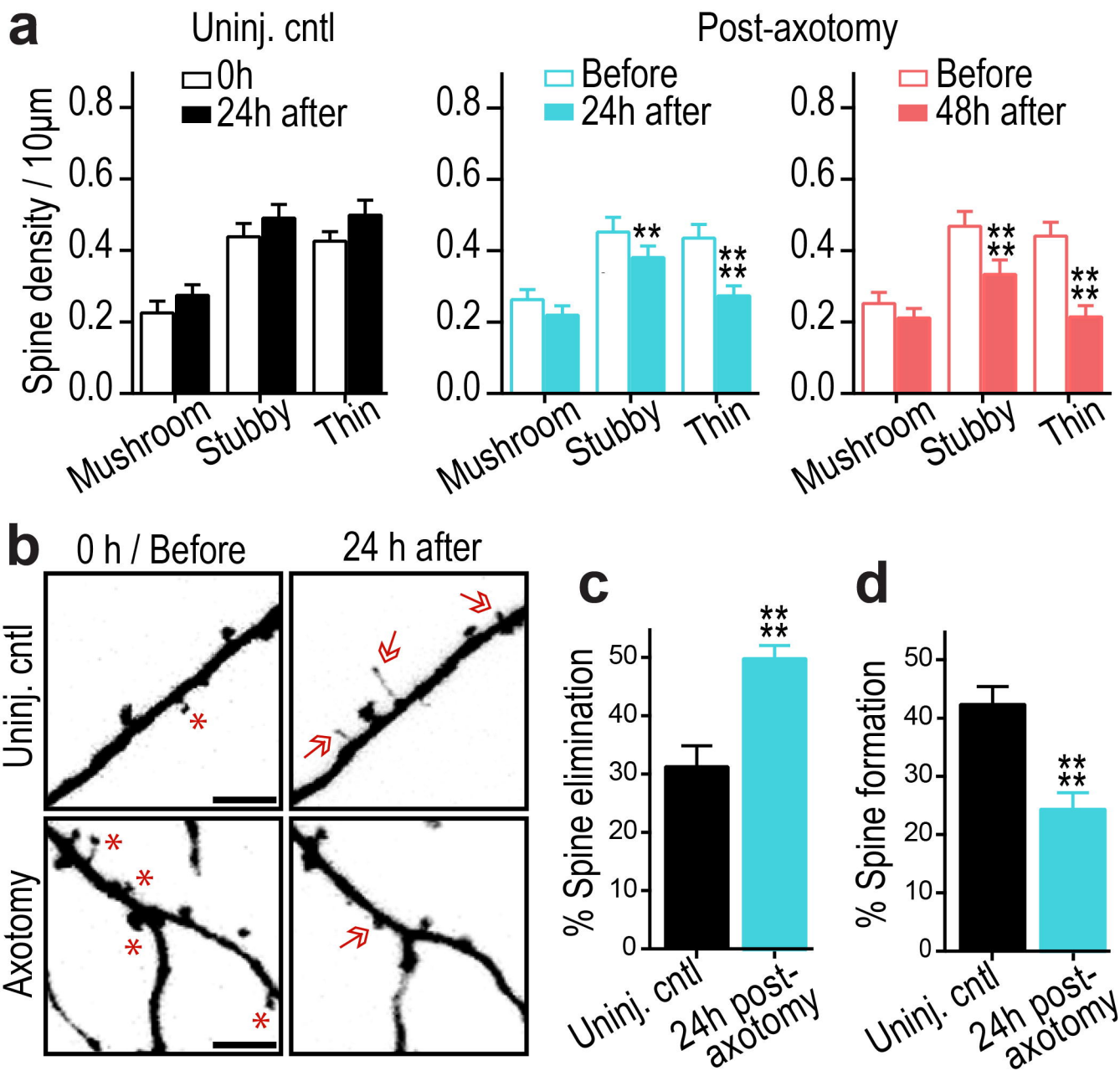
a
Uninj. cntl
0h
24h after
Post-axotomy
Before
24h after
Before
48h after
Spine density / 10µm
0.0
0.2
0.4
0.6
0.8
Mushroom
Stubby
Thin
**
b
0 h / Before
24 h after
Uninj. cntl
Axotomy
c
% Spine elimination
0
10
20
30
40
50
Uninj. cntl
24h post-axotomy
d
% Spine formation

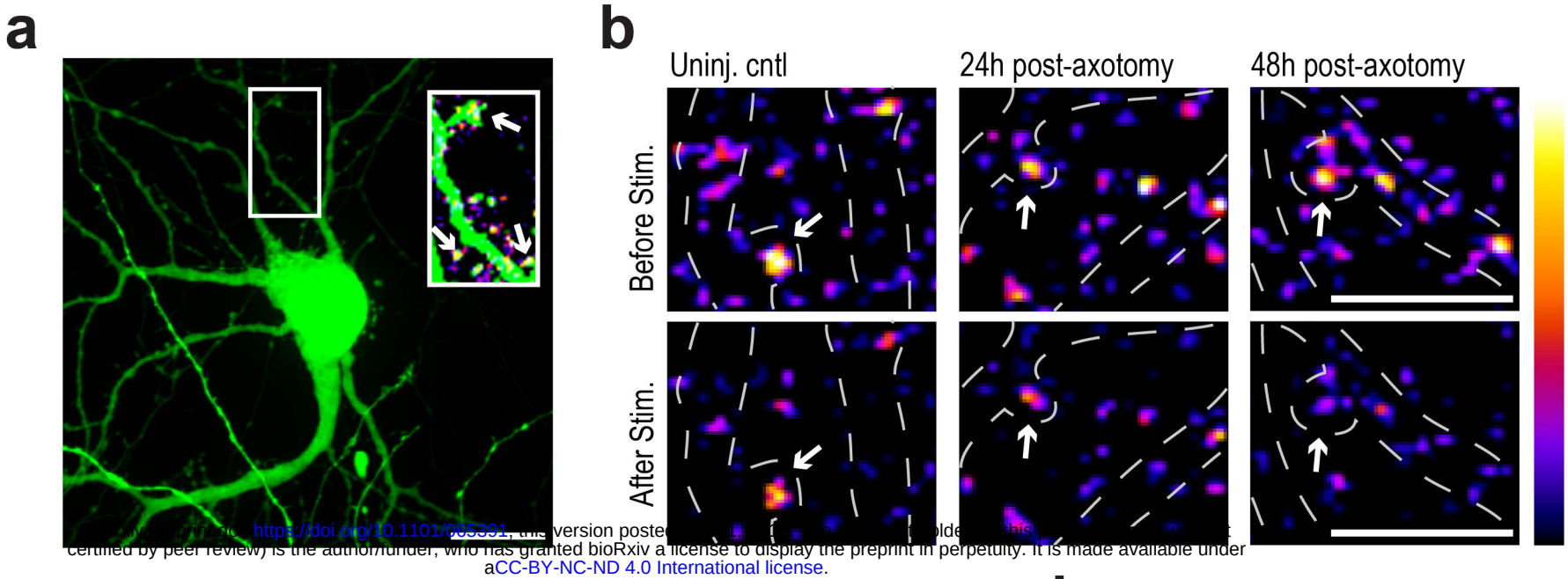

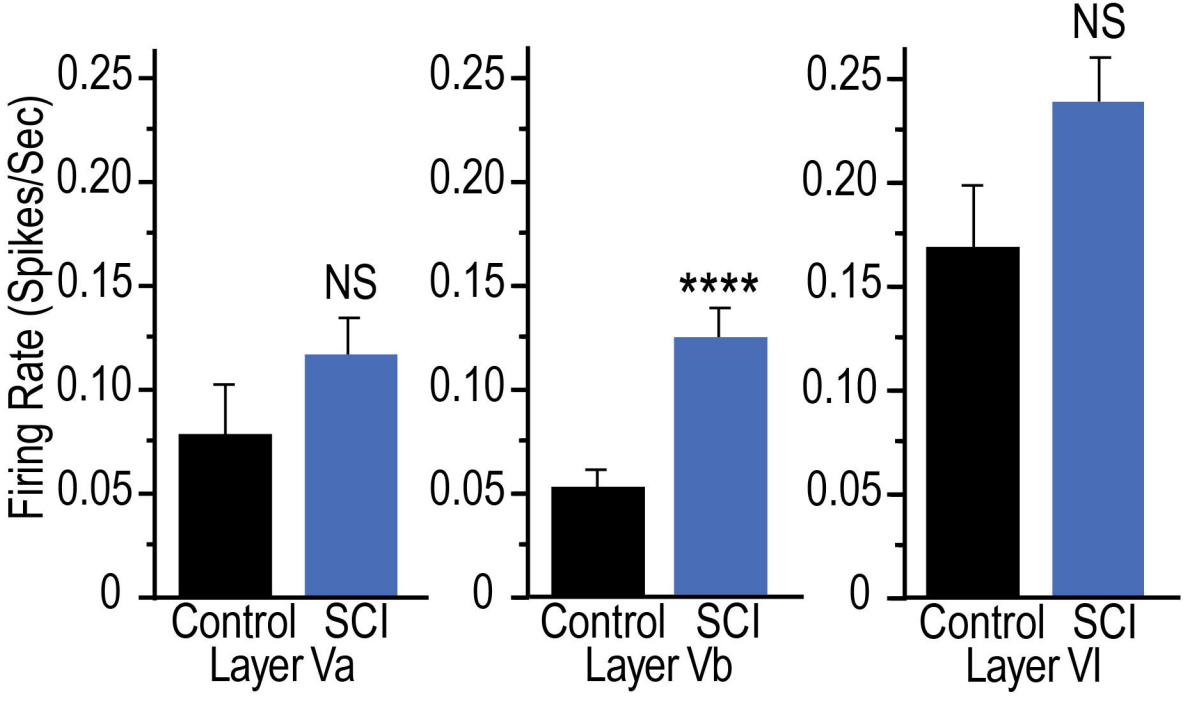
Firing Rate (Spikes/Sec)
0.25
0.20
0.15
0.10
0.05
0
NS
Control
SCI
Layer Va
****
Layer Vb
NS
Layer VI

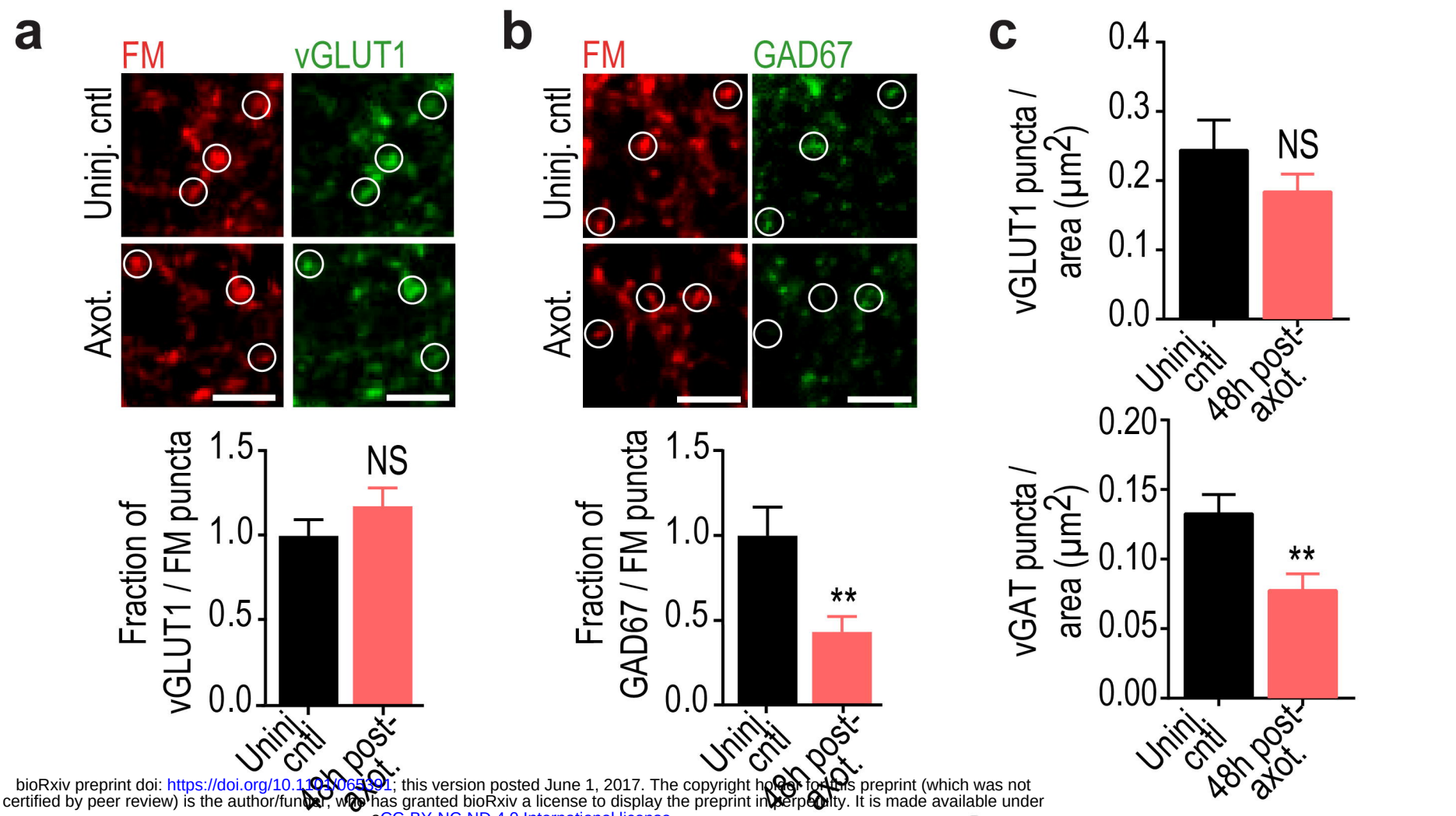

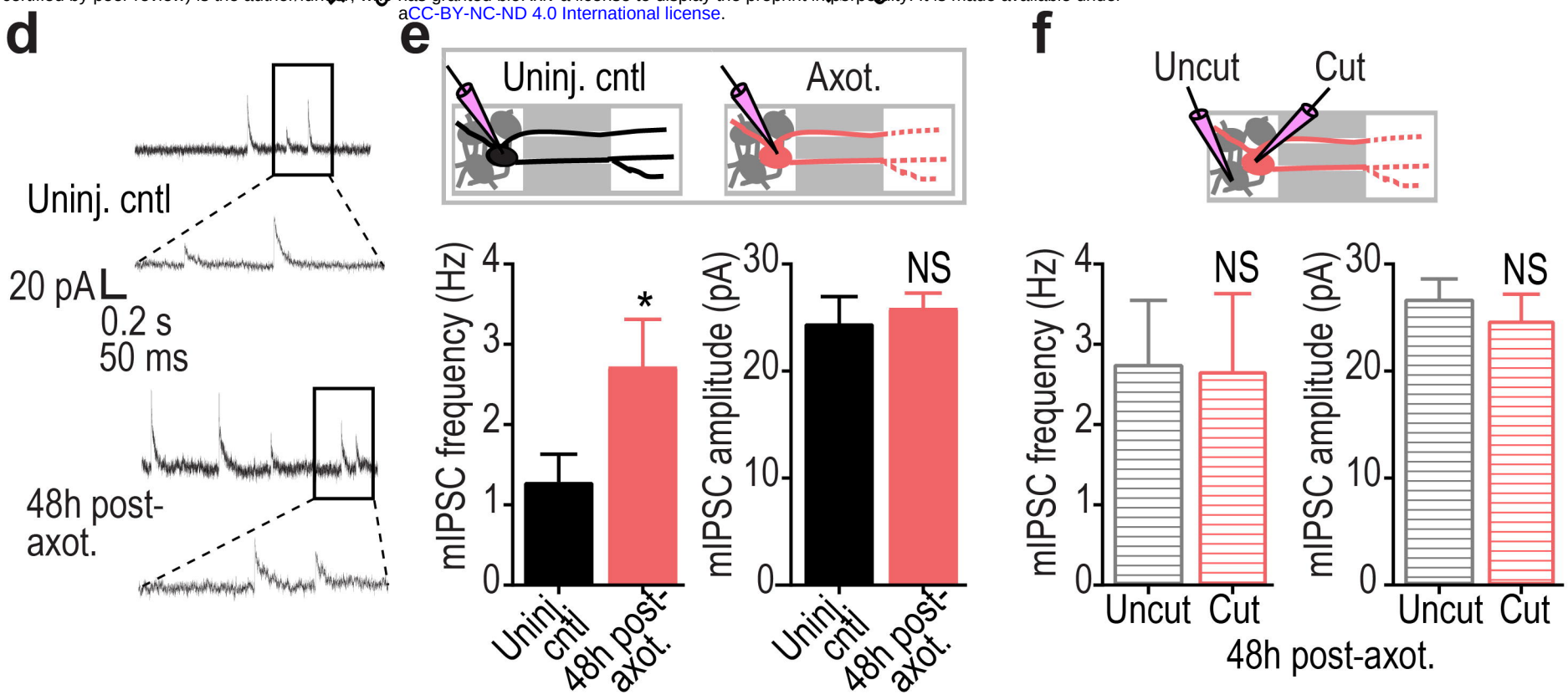

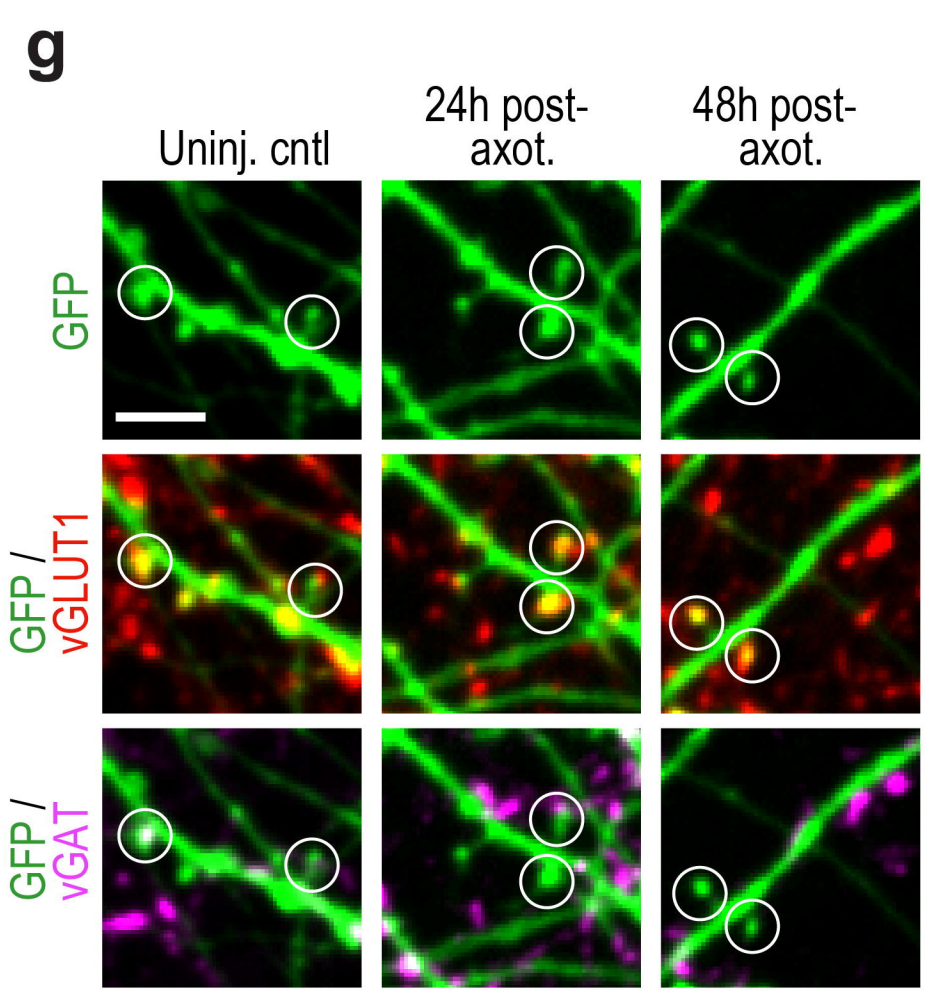

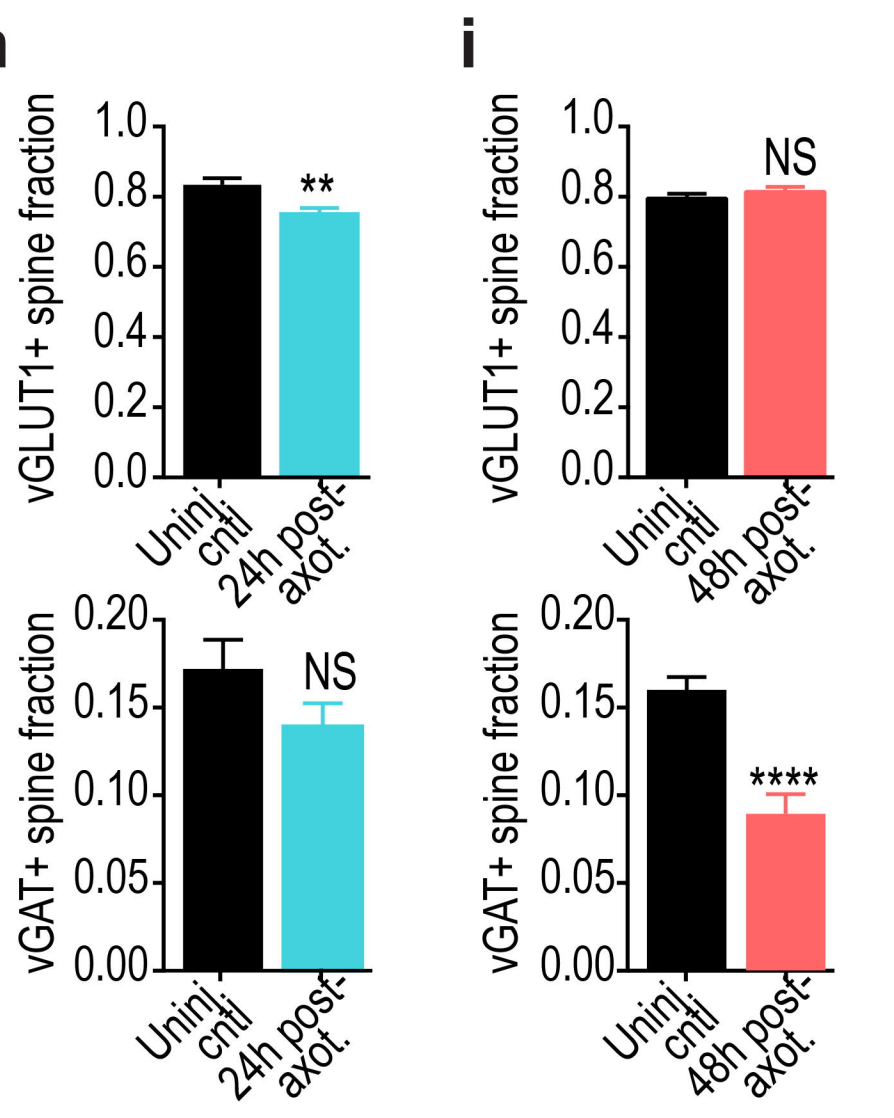

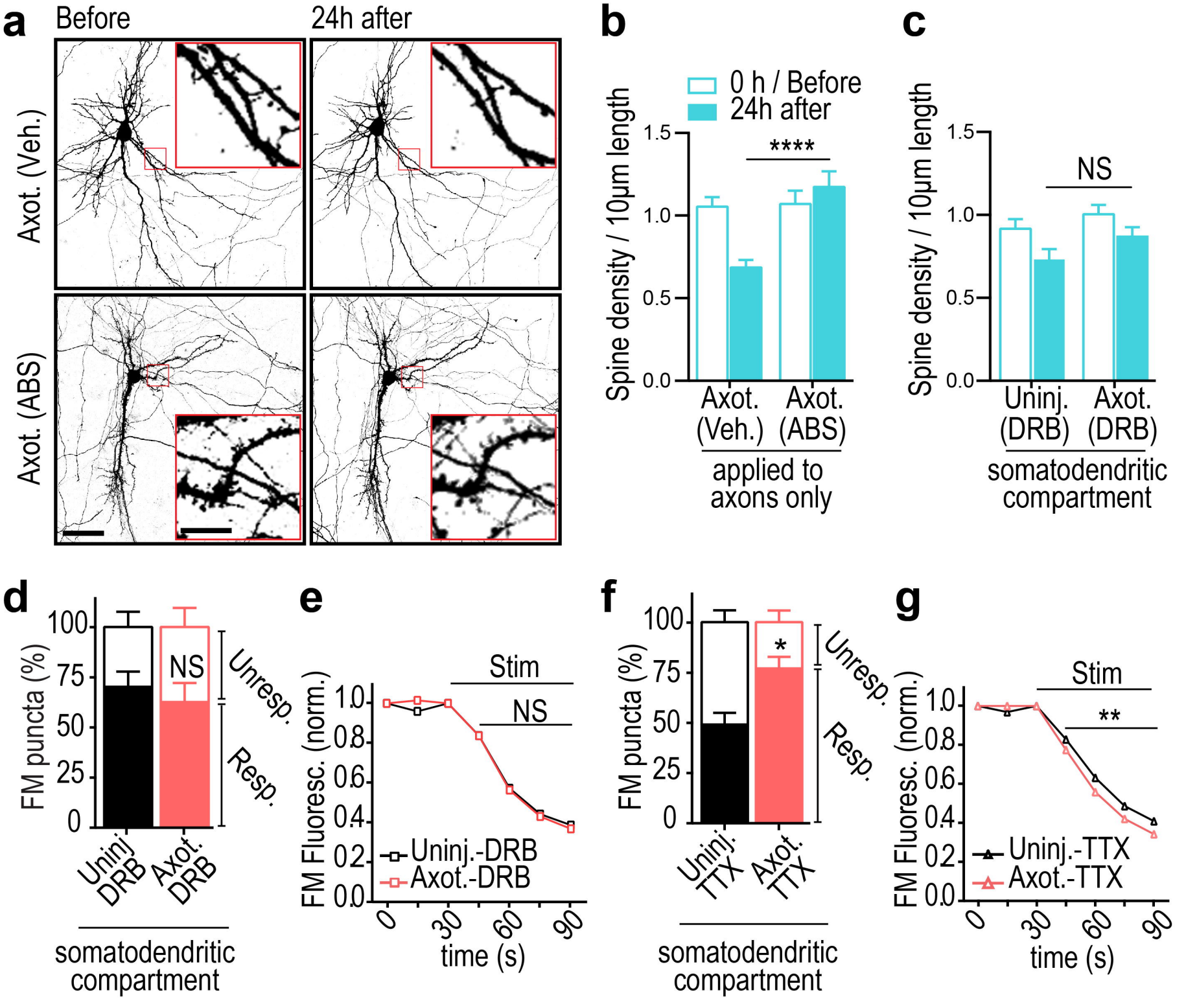
a
Before
24h after
Axot. (Veh.)
Axot. (ABS)
b
0 h / Before
24h after
Spine density / 10µm length
1.5
1.0
0.5
0.0
****
Axot. (Veh.)
Axot. (ABS)
applied to axons only
c
Spine density / 10µm length
1.5
1.0
0.5
0.0
NS
Uninj. (DRB)
Axot. (DRB)
somatodendritic compartment
d
FM puncta (%)
100
75
50
25
0
NS
Unresp.
Resp.
Uninj DRB
Axot. DRB
somatodendritic compartment
e
FM Fluoresc. (norm.)
1.0
0.8
0.6
0.4
0.2
0.0
Stim
NS
Uninj.-DRB
Axot.-DRB
0
30
60
90
time (s)
f
FM puncta (%)
100
75
50
25
0
*
Unresp.
Resp.
Uninj. TTX
Axot. TTX
somatodendritic compartment
g
FM Fluoresc. (norm.)
1.0
0.8
0.6
0.4
0.2
0.0
Stim
**
Uninj.-TTX
Axot.-TTX
0
30
60
90
time (s)